学位論文

Multiphoton ionization of atoms by extreme ultraviolet free electron laser seeded with high-order harmonics of Ti:Sapphire laser and amplification of backward fluorescence in laser induced filaments

(チタンサファイアレーザーの高次高調波によってシードされた極端紫外領域自由電子レーザーによる原子の多光子イオン化およびレーザー誘起フィラメントによる後方蛍光の増幅)

平成 24 年 12 月　博士(理学)申請

東京大学大学院理学系研究科
化学専攻
大和田　成起

Index

Chapter 3

Multiphoton ionization induced by the seeded free-electron laser

Chapter 4

Amplified spontaneous $C^3\Pi_u$ - $B^3\Pi_g$ emission and rotational and vibrational state distributions in $C^3\Pi_u$ state of N_2 in femtosecond laser induced filament in air

Chapter 5

Acknowledgments

Abstract

Chapter 1

Chapter 1 is a general introduction of the generation of the intense pulses in the EUV wavelength region, and the nonlinear optical phenomena in the intense laser field, such as a femtosecond laser induced filament.

Chapter 2

Intense coherent EUV pulses were generated by seeding the SCSS test accelerator at the RIKEN Harima Branch by the 13th order harmonics of Ti:Sapphire laser pulses. The 13th order harmonic pulses were introduced into a couple of undulators, so that they overlapped with electron bunches both temporally and spatially. The arrival timing drift between the 13th high-order harmonic pulses and the electron bunches was monitored by using the electro-optic spectral decoding technique, and the drift was fed back to a trigger delay circuit of the Ti:Sapphire laser system. By correcting the drift, the seeded FEL pulses were produced continuously for long hours.

Chapter 3

Recent advances in FEL technologies in the EUV and X-ray wavelength regions have afforded us opportunities to investigate phenomena occurring when atoms and molecules are irradiated with intense light pulses in the EUV and X-ray wavelength regions. Among the recent achievements in the development of EUV-FELs, the generation of full-coherent EUV-FEL pulses by injecting a high-order harmonic of a Ti:Sapphire laser into the FEL is noteworthy, as was demonstrated by Togashi *et al.* using the SCSS test

accelerator at the RIKEN Harima Branch. In the present study, as a first step in the application of the seeded EUV-FEL pulses to the investigation of responses of atoms and molecules to intense and full-coherent EUV light, we investigate a multiphoton ionization process of He.

Chapter 4

A femtosecond laser-induced filament in air was investigated by detecting the $C^3\Pi_u$ - $B^3\Pi_g$ (0, 0) fluorescence of N_2. The intensity of the backward fluorescence increased exponentially as a function of the filament length, showing the amplification of the spontaneous emission. The vibrational and rotational temperatures of N_2 in the C state determined by spectroscopic analyses were found to take respectively almost the same values of 2800(200) K and 450(100) K in the wide laser intensity range between 0.5 and 6 mJ/pulse, which can be regarded as evidence of the clamping of the laser field intensity in the filament.

Chapter 1

General introduction

1. Introduction

In an intense laser field generated by focusing femtosecond Ti:Sapphire laser pulses in the near infrared (NIR) wavelength region, atoms and molecules show nonlinear responses to the laser field intensity in their ionization and light induced chemical processes. Multiphoton ionization, tunnel ionization, above threshold ionization, Coulomb explosion, and the hydrogen migration leading to the formation of H_3^+ from hydrocarbon molecules [1-3] have been reported as nonlinear optical phenomena occurring in the intense NIR laser field. On the other hand, in the extreme ultraviolet (EUV) wavelength region, the electrons of atoms and molecule are excited to the auto-ionizing states or the super-excited states by one photon absorption, because the photon energy of EUV light is one order of magnitude larger than that of NIR light, breaking and formation of chemical bonds could occur after the photo-excitation of molecules. For example, Xe^{21+} can be formed by irradiating with femtosecond laser pulses at λ = 13 nm generated by using free-electron laser (FEL) [4]. The formation of multiply charged Xe atoms, $Xe^{n+}(n \leq 21)$, shows that as many as 57 photons are absorbed by a Xe atom within the temporal pulse width (10 fs). In the NIR wavelength region, nonlinear optical processes producing such highly charged atomic ions have not been reported. When I started my PhD course, it was time such FEL facilities were being developed in Japan, Europe, and United States, and the intense laser pulses in the EUV and the Soft X-ray wavelength region were becoming available. Because I was interested in responses of atoms and molecules to an intense laser field in the EUV wavelength region, I decided to use SPring-8 Compact self-amplified

spontaneous emission (SASE) Source (SCSS) test accelerator at RIKEN Harima Branch, which is the FEL light source in Japan that became available in those days.

It is true that the SASE-FEL is a powerful light source with which we could investigate nonlinear optical phenomena of atoms and molecules in the EUV and soft X-ray wavelength regions. However, the temporal and spectral profiles of the SASE-FEL pulses exhibit uncontrollable spike-like structures originated from the SASE-FEL light amplification scheme, that is, the temporal coherence of the SASE-FEL pulses are poor. When we investigate nonlinear optical phenomena in an intense laser field, such as multiphoton ionization and tunneling ionization, the temporal coherence within a single pulse needs to be assured. If shot-to-shot fluctuations of the temporal and spectral profiles are large, interpretation of the experimental results becomes very difficult. Therefore, in order to investigate nonlinear optical phenomena, we put a highest priority on the improvement of the temporal coherence of the SASE-FEL pulses.

In Chapters 2 and 3 of the present thesis I describe (i) the generation of full-coherent FEL pulses in the EUV wavelength region by seeding the FEL by the 13th-order harmonic of Ti:Sapphire laser and (ii) the first observation of a two-photon ionization process of He atoms using the high-order harmonic seeded FEL pulses.

While making an effort in improving the temporal coherent of FEL pulses, I became also interested in incoherent spontaneous emission from a femtosecond laser induced filament. When intense femtosecond laser pulses are focused into the transparent media, the pulses propagates by keeping their high intensity and small beam di-

ameter over a long distance [5]. This self-guided propagation of the laser pulse called a femtosecond laser induced filament is achieved by a balance between the self-focusing and the plasma defocusing. Because of this balance, the laser field intensity in the filament is kept almost constant, and this phenomenon is called as intensity clamping [6, 7]. The filament has been regarded as an attractive phenomenon by a variety of its applications such as generation of white light, few-cycle pulses [8, 9], and the third harmonic [10]. The fluorescence emission from electronically excited molecular ions in the filament was also reported [11, 12]. It has been reported [13] that the fluorescence emitting from the femtosecond laser induced filament in the direction opposite to the laser propagation direction increases exponentially as the length of the filament increases. This suggests that a femtosecond laser induced filament can be a gain medium for lasing.

In Chapter 4 of this present thesis, I show that a femtosecond laser induced filament can be a gain medium for lasing, and investigate that the intensity and spectrum of the fluorescence emitted from the filament when the input laser pulse energy is in the range between 0.5 mJ and 6.0 mJ. The spatial distribution of the population of the excited N_2 in the filament was observed, and the fluorescence intensity was simulated with a model calculation based on the one dimensional amplification model for the amplified spontaneous emission. I confirmed that the population inversion placed along the filament is the origin of the optical gain, and the maximum laser field intensity was kept constant with the range of the input pulse energy between 0.5 mJ to 6 mJ, which is consistent with the intensity clamping phenomena characteristic of femtosec-

ond laser induced parents.

In the following sections, I briefly explain how I conducted the research project about the development of the coherent FEL in Chapter 2, the multiphoton ionization of atoms in an intense EUV laser field in Chapter 3, and the research project about the femtosecond laser induced filament in Chapter 4.

2. Intense light source in EUV wavelength region

Ionization of atoms and molecules can be characterized by Keldysh parameter γ, which is the ratio between the oscillating period of the laser field and the tunneling time of the electron passing through the potential which is formed by the interaction between the laser field and the Coulomb potential of atoms and molecules [14]. The Keldysh parameter can also be represented as

$$\gamma = \sqrt{I_P/2U_P}, \quad (1)$$

where I_P denotes the ionization potential, and U_P denotes the pondermotive energy.

The relationship between the wavelength of the input laser pulses and the laser intensity when γ = 0.1, 1.0, and 10 are shown in Fig. 1. When the wavelength is 800 nm, the intensity of 1×10^{14} W/cm^2 is high enough to satisfy $\gamma\sim$ 1 for a hydrogen molecule in the ground state. However, the intensity of 1.5×10^{16} W/cm^2 is needed to achieve $\gamma\sim$ 1 for the laser pulses of the wavelength at 61.5 nm. Such a high intensity in the EUV wavelength region could not be achieved by the synchrotron radiation or the high-order harmonics of Ti:Sapphire laser [15, 16].

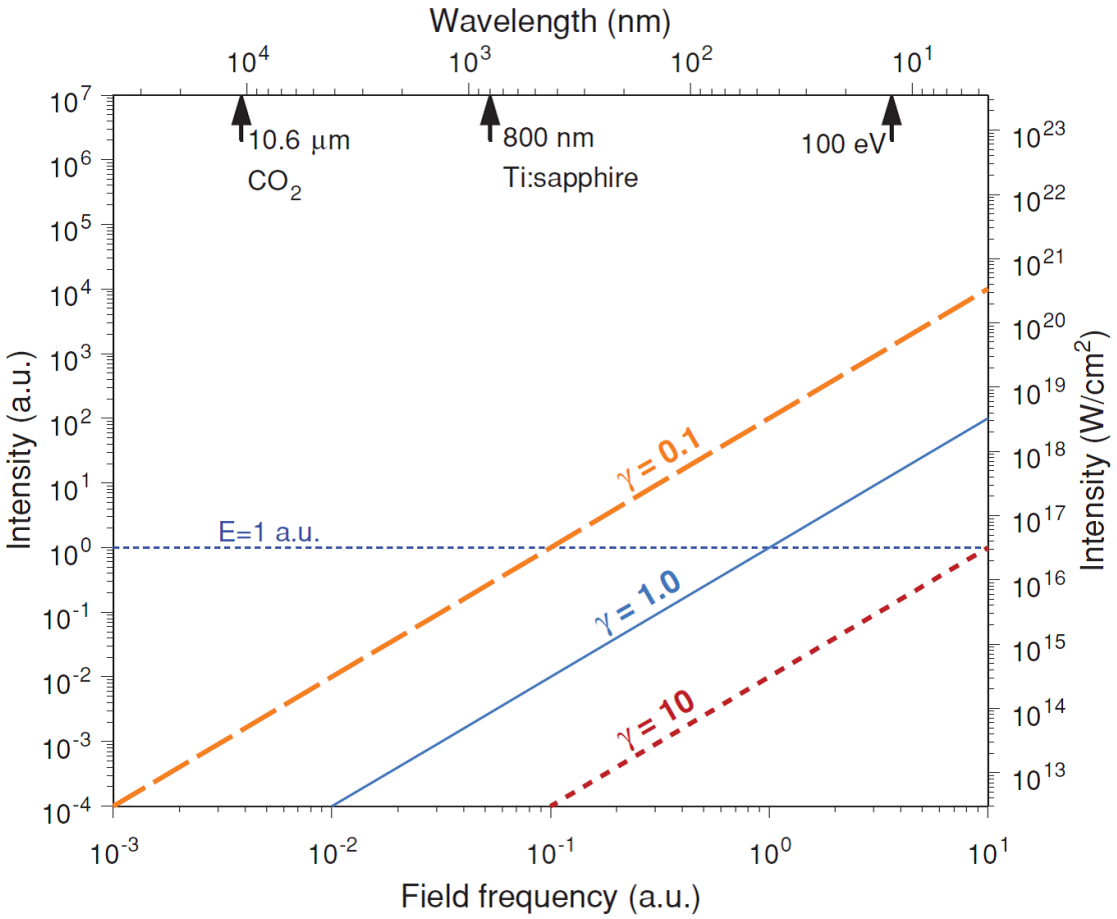

Figure 1. The relationship between the wavelength of the input laser pulses and the laser intensity when the Keldysh parameter is 0.1, 1.0, and 10 [17].

FEL is a promising light source with which we could achieve such a high intensity in the EUV wavelength region. The FEL pulses are generated by strong interaction between relativistic electron bunches and a periodic magnetic field. The spontaneous radiation occurs when electrons accelerated to near the speed of light pass through the periodic magnetic field called an undulator. The wavelength λ of the spontaneous radiation is described as,

$$\lambda = \lambda_u(1 + K^2)/2\gamma^2 , \qquad (2)$$

where λ_u denotes the length of magnetic period composed the undulator, $K =$

$eB_u\lambda_u/2\pi m_e c$ is called the undulator parameter, B_u denotes the peak intensity of the magnetic field in the undulator, e is the electron charge. Depending on the relative phase between the spontaneous radiation and the electron bunch, the electron bunch is accelerated and decelerated. Through this interaction, a longitudinal structure of the electron bunch, which is called micro-bunched electrons, is formed. The micro-bunched electrons radiate at the resonant wavelength λ, and the radiation intensity increases exponentially during passing through the undulator.

The FELs in EUV wavelength region had not been achieved until the SASE-FELs were developed [18, 19]. High density electron bunches with small emittance and small energy spread being introduced into an undulator with high *K*-parameter enables us to achieve the high enough gain to generate intense FEL pulses. In this case, the spontaneous radiations generated at the entrance of the undulator are then amplified through the interaction between electron bunch and the periodical magnetic field.

The spontaneous radiation leading to generate the SASE-FEL pulses is originated from the fluctuation of the longitudinal distribution of the electron bunch, and the pulse-to-pulse intensity fluctuations are uncontrollable. During the propagation of the electron magnetic field through the long undulator together with the electron bunch, its intensity is amplified exponentially by the interaction with an electron bunch. As a consequence the SASE-FEL pulses have random spike-like temporal and spectral structures, and the temporal width and the central wavelength of SASE-FEL pulses are difficult to define. When the SASE-FEL pulses are used as the light source for the excitation and the ionization of atoms and molecules, the analysis of the experimental re-

sults should be difficult. The wavelength dependence and the laser field intensity dependence of the two-photon ionization cross section of He at λ = 53.4, 58.4, 56.0 and 61.4 nm were reported by Sato *et al*. [20], and the strong coupling between the intermediate 1s*n*p resonance state and the $1s^2$ ground state was taken into account. However, there is a limitation to take the coupling into account, because the spectra of the SASE-FEL pulses fluctuated due to the poor temporal coherence. The improvement of the temporal coherence of the SASE-FEL pulses is important for the more precise analysis of the experimental results.

One of the solutions to improve the temporal coherence of the SASE-FEL pulses is the self-seeding. In the self-seeding scheme, a narrow spectral range of the SASE-FEL pulses are selected by a diffractive optics and the selected SASE-FEL pulses are amplified in undulators. The self-seeding method was adopted in the X-ray wavelength religion at the Linac Coherent Light Source (LCLS) [21]. The other solution is the direct seeding, which is the technique to seed the external coherent pulses in the FELs. The coherent seeding pulses are injected into the undulator with the electron bunches, and the seeding pulses induces an initial modulation in the electron bunches, and amplified during passing through the undulator, resulting in the generation of the temporally coherent FEL pulses.

The first demonstration of the direct seeding of the second and the third order harmonics of Ti:Sapphire laser pulses in FEL was performed by DiMauro *et al*. [22].

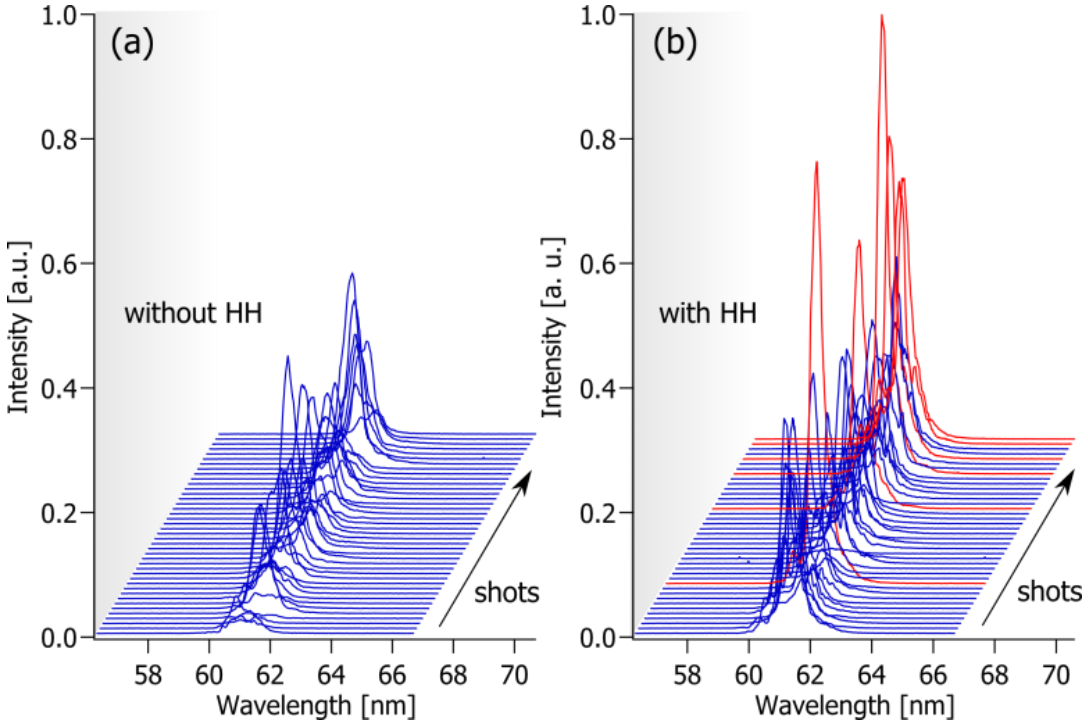

Figure 2. The spectra of (a) the background SASE FEL and (b) the FEL pulse seeded with high order harmonics of Ti:Sapphire laser pulses [24].

Later, the fifth harmonic of Ti: Sapphire laser in the VUV wavelength region (~160 nm) was successfully seeded to FEL at SCSS test accelerator [23]. In 2011, the amplification of the 13th harmonic of Ti:Sapphire laser was achieved in the EUV wavelength region by Togashi and Sato *et al.* [24, 25]. However, since the difference of the arrival time between the electron bunch and 13th order harmonic were fluctuated, it was difficult to generate the seeded FEL pulses for a long time.

3. Free-electron laser seeded by high-order harmonics of Ti:Sapphire laser

In the previous study reported by Togashi *et al.*, the temporal overlap was measured by using a streak camera. Since the 13th harmonic and electron bunch was interrupted to

introduce into the undulator during the measurement of the arrival time, we could not know that the temporal overlap was still realized during the amplification of the 13th harmonic. The arrival timing difference between the electron bunch and the 13th harmonic, which was originated from the variation of the temperature in our experimental environment, reached in the range between 30 and 40 ps within 8 hours.

In order to overcome this problem, a real-time arrival time monitor was required for the application of the high order harmonics. In this thesis, a real-time monitor for the measurement of the arrival time difference between the electron bunch and the 13th harmonic was introduced by using spectrally decoding electro-optic technique. As a result, the difference of the arrival time between the electron bunch and the 13th order harmonic was kept within 1 ps by adjusting the delay time of the 13th order harmonic. As shown in Fig. 3, the 13th order harmonic was amplified up to 20 μJ/pulse.

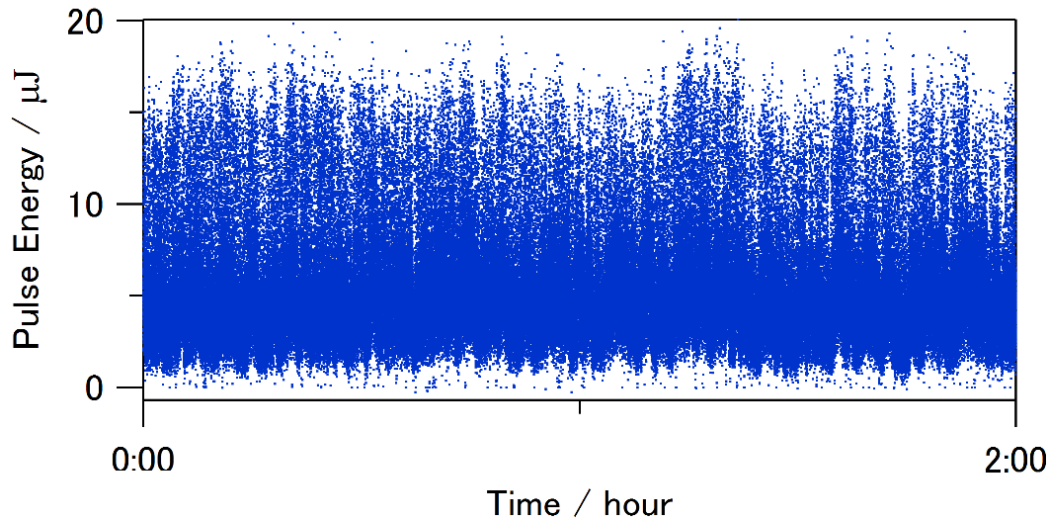

Figure 3. The single shot pulse energy of the FEL when the seeding 13th order harmonic pulses were introduced into the undulators

The FEL seeded by 13th order harmonic of Ti:Sapphire laser pulse was introduced in Chapter 2. In Chapter 3, as the first step of the application of the seeded EUV-FEL pulses to the investigation of responses of atoms and molecules to intense and coherent EUV light, I investigate a two-photon ionization process of He atoms.

4. Fluorescence emitted from femtosecond laser induced filament

The femtosecond laser induced filament in air is formed by a balance between the self-focusing and defocusing of laser light in the plasma generated through the ionization of atoms and molecules in air [26 - 29]. The intensity dependent refractive index n is described as the summation of the linear refractive index n_0 and the nonlinear refractive index n_2 multiplied by the laser intensity I. The reported value of n_2 is positive for air at λ = 800 nm ($n_2 = 4\times10^{-19}$ cm^2/W [30]), n_2I becomes significant in n when the intensity increases. In the case of the Gaussian beam, the spatial distribution of the refractive index in the beam path is also Gaussian, and the medium works as a convex lens. As a consequence the beam is focused, and this phenomenon is called self-focus. The intense laser pulses induce multiphoton or tunneling ionization of atoms and molecules in medium, and generate plasma. The plasma formation decreases refractive index by the density of free electron ρ divided by the twice of the critical plasma density ρ_C above which the plasma becomes over dense and opaque (for example, $\rho_C = 1.7\times10^{21}$ cm^{-3} in air at λ = 800 nm [31]). This reduction of the refractive index induces the divergence of the beam. Because of this balance, the high laser-field intensity in the filament tends to be constant as long as the input laser intensity surpasses a certain

threshold for generating a filament [32, 33]. In Fig. 4, the image of the filament was shown when the input pulse energy was in the range between 1 mJ to 6 mJ. As seen in Fig. 4, the filament length tends to increase as the laser pulse energy increases.

By recording the fluorescence spectra of laser induced filaments in air, Talebpour *et al.* showed that the fluorescence emits from the electronically excited N_2 and N_2^+ [11, 12]. Based on the measurements of the fluorescence of the $C^3\Pi_u$ - $B^3\Pi_g$ (0, 1) transition of N_2 at 357 nm, Luo *et al.* found that the intensity of the fluorescence propagating in the direction opposite to the laser propagation direction increased exponentially as a function of the filament length [13]. In their study, the filament length was assumed as the distance between the self-focus and the geometrical focus, and the filament plasma was assumed as the uniformly excited gain medium. Based on those assumptions, the optical gain of the backward fluorescence emitted from the femtosecond filament was reported for the first time. However, those assumptions did not represent the population distribution of the excited N_2 in the filament correctly.

I investigated about the femtosecond laser filament as the gain medium in this thesis. The schematic drawing of the femtosecond laser filament and the backward fluorescence was shown in Fig. 5. In order to explain the exponential increase in the intensity of the backward fluorescence, I adopted a one-dimensional model for the amplified spontaneous emission (ASE). In order to investigate excitation processes of molecules in the filament, the population distributions in the vibrational and the rotational levels of N_2 in the C state were investigated by the spectroscopic analyses of the fluorescence emitted from the filament. In Chapter 4, I introduce my study on the flu-

orescence emission from the femtosecond laser induced filament.

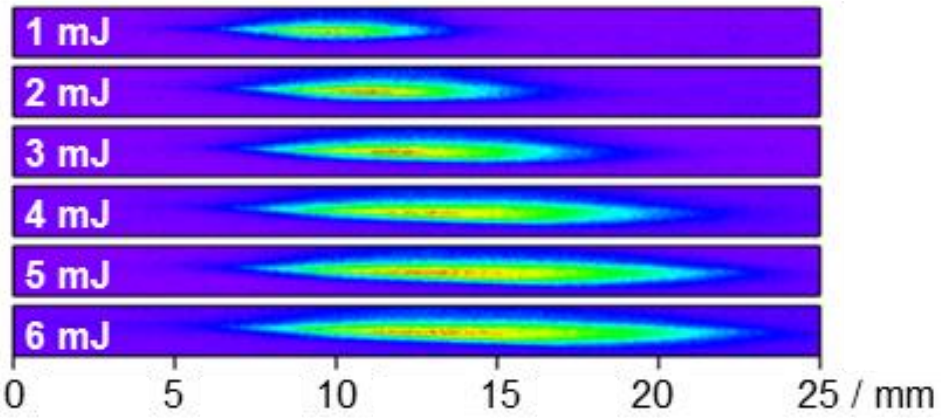

Figure 4. The image of the filament when the input pulse energy was in the range between 1.0 mJ to 6.0 mJ.

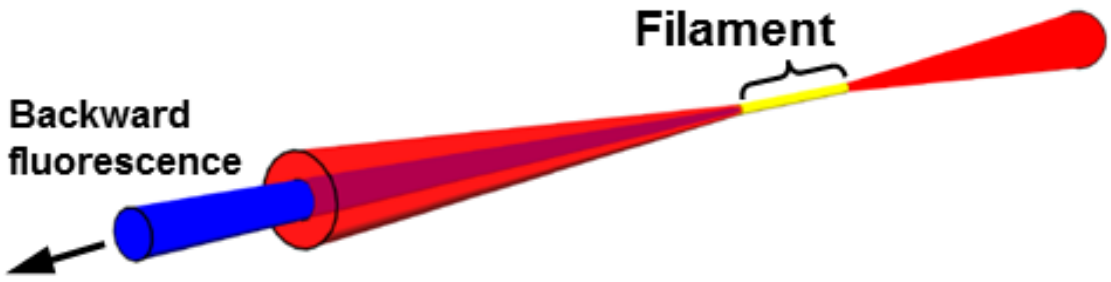

Figure 5. The schematic drawing of the femtosecond laser induced filament ant the backward fluorescence.

References

[1] Y. Furukawa, K. Hoshina, K. Yamanouchi, and H. Nakano, *Chem. Phys .Lett.*, **414**, 117 (2005).

[2] T. Okino, Y. Furukawa, P. Liu, T. Ichikawa, R. Itakura, K. Hoshina, K. Yamanouchi, and H. Nakano, *Chem. Phys. Lett.*, **419**, 223 (2006).

[3] K. Hoshina, Y. Furukawa, T. Okino, and K. Yamanouchi, *J. Chem. Phys.*, **129**, 104302 (2008).

[4] A. A. Sorokin, S. V. Bobashev, T. Feigl, K. Tiedtke, H. Wabnitz, and M. Richter, *Phys. Rev. Lett.*, **99**, 213002 (2007).

[5] A. Braun, G. Korn, X. Liu, D. Du, J. Squier, and G. Mourou, *Opt. Lett.*, **20**, 73 (1995).

[6] A. Becker, N. Akozbek, K Vijayalakshmi, E. Oral. C. M. Bowden, and S. L. Chin, *Appl. Phys. B*, **73**, 287 (2001).

[7] J. Kasparian, R. Sauerbery, and S. L. Chin, *Appl. Phys. B*, **71**, 877 (2000).

[8] C. P. Hauri, W. Kornelis, F. W. Helbing, A. Heinrch, A. Couairon, A. Mysyrowicz, J. Biegert, and U. Keller, *Appl. Phys.* B, **79**, 673 (2004).

[9] C. P. Hauri, A. Guandalini, P. Eckle, W. Kornelis, J. Biegert, and U. Keller, *Opt. Express*, **13**, 7541(2005).

[10] F. Theberge, Q. Luo, W. Liu, S. A. Hosseini, M. Sharifi, and S. L. Chin, *Appl. Phys. Lett.*, **87**, 081108 (2005).

[11] A. Talebpour, M. A-. Fattah, A. D. Bandrauk, and S. L. Chin, *Laser Phys.*, **11**, 68 (2001).

[12] A. Talebpour, S. Petit, and S. L. Chin, *Opt. Commun.*, **171**, 285 (1999).

[13] Q. Luo, W. Liu, and S. L. Chin, *Appl. Phys. B*, **76**, 337 (2003).

[14] L. V. Keldysh, *Soviet Physics JETP*, **20**, 1307 (1965).

[15] E. J. Takahashi, Y. Nabekawa, M. Nurhuda, and K. Midorikawa, *J. Opt. Soc. Am. B.*, **20**, 158 (2003).

[16] E. J. Takahashi, H. Hasegawa, Y. Nabekawa, and K. Midorikawa, *Opt. Lett.*, **5**, 507 (2004).

[17] H. R. Reiss, *Phys. Rev. A*, **82**, 023418 (2010).

[18] K. J. Kim, *Phys. Rev. Lett*., **57**, 1871 (1986).

[19] J. B. Murphy, and C. Pellegrini, *Nucl. Instrum. Methods Phys. Res. A*, **237**, 159 (1985).

[20] T. Sato, A. Iwasaki, K. Ishibashi, T. Okino, K. Yamanouchi, J. Adachi, A. Yagishita. H. Yazawa, F. Kannari, M. Aoyama, K. Yamakawa, K. Midorikawa, H. Nakano, M. Yabashi, M. Nagasono, A. Higashiya, and T. Ishikawa, *J. Phys. B*, **44**, 161001 (2011).

[21] J. Amann, W. Berg, V. Blank, F. -J. Decker, Y. Ding, P. Emma, Y. Feng, J. Frisch, D. Fritz, J. Hastings, Z. Huang, J. Krzywinski, R. Lindberg, H. Loops, A. Lutman, H. -D. Nuhn, D. Ranter, J. Rzepia, D. Shu, Yu. Shvyd'ko, S. Spampinati, S. Stoupin, S. Terentyev, E. Trankhtenberg, D. Waltz, J. Welch, J. Wu, A. Zholents, and D. Zhu, *Nat. Photn.*, **6**, 693 (2012).

[22] L. DiMauro, A. Doyuran, W. Graves, R. Heese, E.D. Johnson, S. Krinsky, H. Loos, J. B. Murphy, G. Rakowsky, J. Rose, T. Shaftan, B. Sheehy, J. Skaritka, X. J. Wang,

and L. H. Yu, *Nucl. Instrum. Methods in Phys. Res. A*, **507**, 15 (2003).

[23] G. Lambert, T. Hara, D. Garzella, T. Tanikawa, M. Labat, B. Carre, H. Kitamura, T. Shintake, M. Bougeard, S.Inoue, Y. Tanaka, P. Salieres, H. Merdji, O. Chubar, O. Gobert, K. Tahara, and M.-E. Couprie, *Nat. Phys.*, **4**, 296 (2008).

[24] T. Togashi, E. J. Takahashi, K. Midorikawa, M. Aoyama, K. Yamakawa, T. Sato, A. Iwasaki, S. Owada, T. Okino, K. Yamanouchi, F. Kannari, A.Yagishita, H. Nakano, M. E. Couprie, K. Fukami, T. Hatsui, T. Hara, T. Kameshima, H. Kitamura, N. Kumagai, S. Matsubara, M. Nagasono, H. Ohashi, T. Ohshima, Y. Otake, T. Shintake, K. Tamasaku, H. Tanaka, T. Tanaka, K. Togawa, H. Tomizawa, T. Watanabe, M. Yabashi, and T. Ishikawa, *Opt. Express*, **19**, 317 (2011).

[25] T. Sato, A. Iwasaki, S. Owada, K. Yamanouchi, K. Midorikawa, M. Aoyama, K. Yamakawa, T. Togashi, K. Fukami, T. Hatsui, T. Hara, T. Kameshima, H. Kitamura, N. Kumagai, S. Matsubara, M. Nagasono, H. Ohashi, T. Ohoshima, T. Shintake, K. Tasamasku, H. Tanaka, T. Tanaka, K. Togawa, H. Tomizawa, T. Watanabe, M. Yabashi, T. Ishikawa, *J. Phys. B*, **46**, 164006 (2013).

[26] H. R. Lange, G. Grillon, J. -F. Ripoche, M. A. Franco, B. Lamouroux, B. S. Prade, and A. Mysyrowicz, *Opt. Lett.*, **23**, 120 (1998).

[27] B. La. Fontaine, F. Vidal, Z. Jinag, C. Y. Chien, D. Comtois, A. Desparois, T. W. Johnston, J. -C. Kieffer, and H. Pepin, *Phys. Plasmas*, **6**, 1615 (1999).

[28] S. L. Chin, *Femtosecond Laser Filamentation*, Springer, New York (2010).

[29] S. L. Chin, T -J. Wang, C. Marceau, J. Wu, J. S. Liu, O. Kosareva, N. Panov, Y. P. Chen, J. -F. Daigle, S. Yuan, A. Azarm, W. W. Liu, T. Seideman, H. P. Zeng, M.

Richardson, R. Li, and Z. Z. Xu, *Laser Phys.*, **22**, 1 (2012).

[30] E. T. J. Nibbering, G. Grillon, M A. Franco, B. S. Prade, and A. Mysyrowicz, *J. Opt. Soc. Am. B*, **14**, 650 (1997).

[31] A. Couairon, and A. Mysyrowicz, *Phys. Rep.*, **441**, 47 (2007).

[32] A. Becker, N. Akozbek, K Vijayalakshmi, E. Oral. C. M. Bowden, and S. L. Chin, *Appl. Phys. B*, **73**, 287 (2001).

[33] J. Kasparian, R. Sauerbery, and S. L. Chin, *Appl. Phys. B*, **71**, 877 (2000).

Chapter 2

Extreme ultraviolet free-electron laser seeded by high order harmonics of Ti:Sapphire laser

1. Introduction

1.1. Free-electron laser seeded by coherent eternal laser

Spontaneous radiation occurs when electrons accelerated near the speed of light pass through a periodic magnetic field called an undulator or wiggler. The wavelength λ of the spontaneous radiation is described as

$$\lambda = \lambda_u(1 + K^2)/2\gamma^2 , \quad (1)$$

where λ_u denotes the length of the magnetic period of the undulator, $K = eB_u\lambda_u/2\pi m_e c$ with e being the elementary charge is the averaged undulator parameter, B_u denotes the peak intensity of the magnetic field in the undulator. The undulator parameter signifies the deflection angle of the electrons and the divergence of the synchrotron radiation. The divergence of the emission is defined by $1/\gamma$, and $\gamma = E/m_e c^2$is is called the relativistic factor, where E is the electron energy and m_e is the electron mass. Equation (1) exhibits the wavelength tunability of free-electron lasers (FEL) and the possibility of generating optical pulses in short wavelength regions such as the extreme ultraviolet (EUV) and X-ray regions as the electron kinetic energy reaches over 200 MeV (or 99.999 % of the speed of light) and the K parameter becomes larger than 1. The spontaneous radiation is amplified through the propagation in the undulator with an electron bunch. Since there is currently no suitable optics to construct an oscillator in the EUV or X-ray wavelength region, the single-pass amplification of the spontaneous emission is a promising way to generate intense pulses in a short wavelength region. This scheme is called the self-amplified spontaneous emission (SASE) [1, 2].

However, both the spectral profile and the temporal profile of SASE-FEL pulses exhibit uncontrollable spike-like structures and these structures change

shot-by-shot due to the spontaneous radiation generated at the entrance of the undulator. The peak power of FEL pulses with a single-peak structure should be larger than that of FEL pulses with a multi-peak structure. Thus the improvement of the temporal coherence of SASE-FEL pulses is one approach to generate a strong laser field in the EUV or X-ray wavelength region. Seeding the FEL with a coherent external laser is a promising approach to improve the coherence of the FEL pulses. Direct seeding of the FEL with high order harmonics generated in gases [3, 4] is one approach to generate intense coherent pulses in the short wavelength region. This direct seeding technique was demonstrated at the Brookhaven National Laboratory by L. DiMauro *et al*. [5]. They generated the second and the third harmonic of the Ti:Sapphire laser pulse, and the pulse energy of the seeded FEL were 10 μJ, which was about 1000 times larger than the pulse energy of the corresponding SASE-FEL. In 2008, the seeding of FEL using the 5th order harmonics of Ti:Sapphire laser was performed at the SCSS test accelerator in the RIKEN Harima Branch [6]. The seeding pulses at λ = 160 nm were amplified from 0.53 nJ to 4.3 nJ in the undulator.

The development of high order harmonics of ultrashort laser pulses in the decade was remarkable and their intensities in the EUV or the soft X-ray wavelength regions has recently become much higher [7 - 9]. The intensity of the 13th order harmonic of Ti:Sapphire laser has reached the order of 10 kW, which is about 100 times larger than the spontaneous radiation emitted at the entrance of the first undulator. Direct seeding in EUV is feasible when the intense high-order harmonic light source is combined with the FEL. Togashi *et al.* demonstrated this first in the EUV wavelength region at the SCSS test accelerator in the RIKEN Harima Branch [10]. The pulse energy of 13th order harmonic pulses at λ = 61.2 nm was amplified from 2 nJ to 1.3 μJ,

while the number of the seeded FEL pulses with respect to the total number of FEL pulses was only 0.2 % of the total number of shots. This meant that it was difficult to use the seeded FEL pulses in our application experiments such as the measurement of the time of flight mass spectrometry of gaseous atoms and molecules. The reason for the small number of shots of the amplified pulses was mainly due to the poor temporal overlap between the electron bunches and the 13th order harmonic pulses. For the seed FEL amplification the temporal, spatial and the spectral overlap between the electron bunch and the seed laser pulse are important. Since the temporal width of the electron bunch and 13th order harmonic pulse were less than 1 ps and 50 fs, respectively, the temporal overlap was required at an accuracy level of sub-ps. However, the arrival time difference between the electron bunch and the seeding laser pulse varied rapidly as shown in Fig. 1, and the drift of the arrival time difference reached the range between 30 and 40 ps within 8 hours.

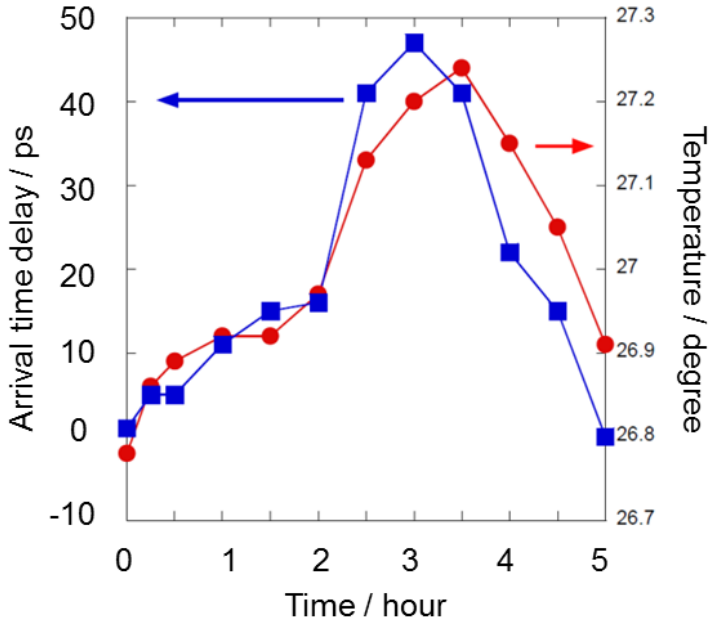

Figure 1. The variation of the arrival time drift (blue line) and the temperature of the SCSS facility (red line) [12].

The variation of the arrival time difference were quite large to keep the temporal overlap between the electron bunch and the seeding laser pulse, and the improvement of the temporal overlap was desired to keep the direct seeding of the high-order harmonic in the FEL for long time.

The temporal overlap was measured by using a fast streak camera (Hamamatsu Photonics, FESCA-200) in the previous experiment reported by T. Togashi *et al*. The optical transition radiation (OTR) [11] generated when the electron bunch hit the thin gold plate (mirror) and the reflection of the seeding laser pulses from the gold plate were introduced into the streak camera. Since this scheme was a destructive scheme, the arrival time could not be measured during the amplification of the seeding laser. In order to keep the temporal overlap for long time, a non-destructive arrival time monitor was needed to measure the arrival time difference during the amplification of the seeding laser. In the present study, we decided to adopt the electro-optic (EO) sampling technique.

1.2. Arrival time measurement based on EO sampling

The EO sampling technique has been widely used to characterize an electrical waveform in the terahertz (THz) region [13 - 15]. The electric field generated by the relativistic electron bunch corresponds to a half-cycle of the THz wave, and the EO sampling technique has been applied to measure the longitudinal profile and the arrival time of the electron bunch. The linearly polarized THz pulse induces birefringence in the EO crystal. The relative phase retardation between the two components propagating along the optical axis and the other axis is given by

$$\Gamma = \frac{2\pi}{\lambda} {n_0}^3 r_{41} E \, . \tag{2}$$

If the co-propagating probe pulse is injected into the EO crystal at the moment when the electron bunch passes by the EO crystal, the phase retardation is induced by the electric field generated by the electron bunch. The phase retardation is converted into an intensity modulation of the probe pulse after passing through a polarizer whose axis is perpendicular to the initial polarization of the probe pulse. The EO sampling technique can be classified into four types: scanning delay sampling, spatial decoding, spectral decoding, and temporal decoding. These methods are used to encode the temporal structure of the Coulomb field of the spatially and temporally compressed charges in the order of 0.4 nC in the electron bunch, and decoded in several ways.

The scanning delay sampling method was the simplest EO sampling method to detect an electron bunch. The schematic of scanning delay sampling is shown in Fig. 2. Probe pulses with a short temporal width was used to detect the intensity modulation at the fixed part of the electron bunch. By scanning the optical delay between the probe laser and the electron bunch, the temporal profile of the electron bunch is obtained as an ensemble average. Since this method is not a single shot measurement, the temporal resolution suffers from the arrival time jitter between the probe laser pulse and the electron bunch, and not for the real time monitor because of the low reputation rate of the accelerator. X. Yan *et al*. measured the temporal profile of the electron bunch whose temporal width was 1.7(2) ps with a sub-ps time resolution at FELIX FEL in 2000 [16].

The spatially decoding technique is to measure the arrival time as the position at the EO crystal, imaged onto the detector. The schematic of this decoding is shown in Fig. 3. This scheme was demonstrated at SLAC [17], and FLASH [18].

The spectrally decoding EO sampling technique uses the linearly chirped pulse as a probe pulse. The schematic of this method is shown in Fig. 4. The ultrashort

probe laser pulse at 800 nm was introduced into dispersive media, and then temporally stretched. The polarization of the probe pulse is cleaned by a high extinction polarizer. Then the probe pulse was introduced into the EO crystal. As the electron bunch passes by the EO crystal, the Columbic field induces birefringence in the EO crystal where the part of the probe pulse was retarded. After the probe laser pulse passes through the EO crystal and the polarizer, the probe pulse is detected by a spectrometer. Since the probe pulse is linearly chirped, the relationship between the time and the frequency of the probe pulse is linear. The spectral modulation is converted into temporal modulation, which corresponds to the temporal profile of the Coulomb field induced by the electron bunch. The spectrally decoding EO sampling measurement was applied to an arrival time monitor and an electron bunch measurement at FELIX [19, 20].

The temporal resolution T_{min} of the spectrally decoding technique is described as follows [14, 21],

$$T_{min} = \sqrt{T_C T_0}\,, \tag{3}$$

where T_C is the temporal width of the chirped probe pulse and T_0 is the temporal width of the probe pulse in the Fourier transform limit. For example, in our experiment, the Fourier transform limit duration of the seeding laser pulse was 150 fs and the seeding laser pulse was stretched up to 10 ps. The temporal resolution was about 1.3 ps. Since the temporal duration of the electron bunch used in this experiment was about 600 to 700 fs, which was below the temporal resolution, the resulting EO signal could not represent the temporal profile of the exact temporal profiles of the electron bunch. To improve the temporal resolution in the spectral decoding method, the probe pulse with a broadband spectrum and a small chirp rate, which correspond to small T_0 and T_C, have to be used. The group velocity mismatch between the THz wave generated by the

electron bunch and the probe laser pulse is not negligible when the probe pulse has a broadband spectrum. If the chirp rate becomes smaller, the time window of EO sampling measurement becomes narrower. A narrower time window means limited sampling time for the EO measurement as an arrival time monitor. A better temporal resolution is obtained by a temporally decoding EO sampling technique, which is based on cross correlations of the chirped pulse and the short pulse.

The temporally decoding EO sampling method was invented by G. Berden *et al*. They separated a laser pulse into two, of which one was chirped and introduced into an EO crystal. The rest of the pulse and chirped pulse were sent to a non-linear crystal. A single shot cross correlation was measured between two pulses to detect an intensity modulation of the chirped pulse in the temporally decoding method. They measured the temporal width of the electron bunch whose temporal width was 650 fs. They used 30 fs and 21 ps probe pulses, and detected the EO signal lasting for 460 fs [22].

In this thesis, a non-destructive and real-time monitor based on the electro-optic spectrally decoding technique was constructed. The arrival time difference was calculated from the variation of the peak position of the spectra of the EO signal, and fed back to a trigger delay circuit of the seeding laser system by the home-built program. Then the arrival time fluctuations were kept in the order of sub-ps for a long time. The seeded FEL pulses at λ = 61.5 nm with a pulse energy of 20 μJ at the maximum were generated. This allows the seeded FEL to be applied to experiments in intense laser fields.

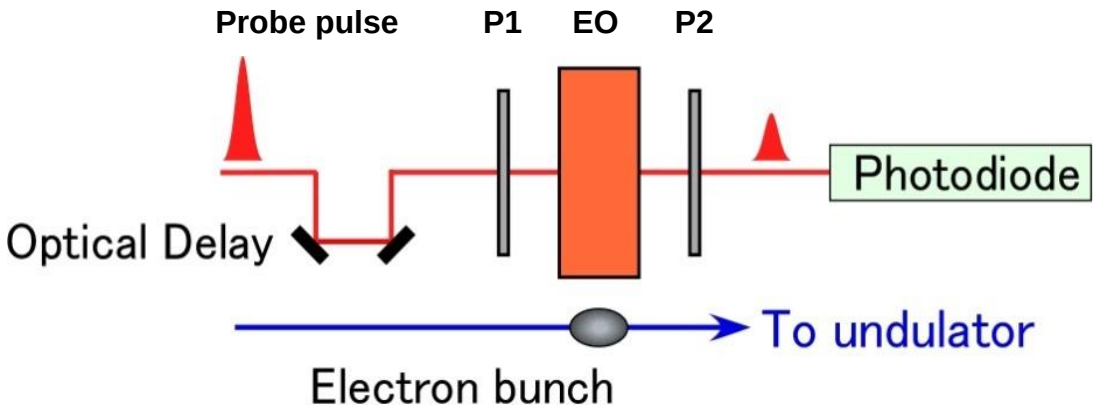

Figure 2. The schematic of the scanning delay sampling method. The probe pulse transmits the polarizer P1 and the EO crystal and the phase retardation occurs. The phase retardation is changed into an intensity change by polarizer P2 and detected by a photodiode. The polarizer P1 and P2 are in crossed-Nicol. By changing the optical delay, the different positions of the electron bunch is probed for each electron bunch.

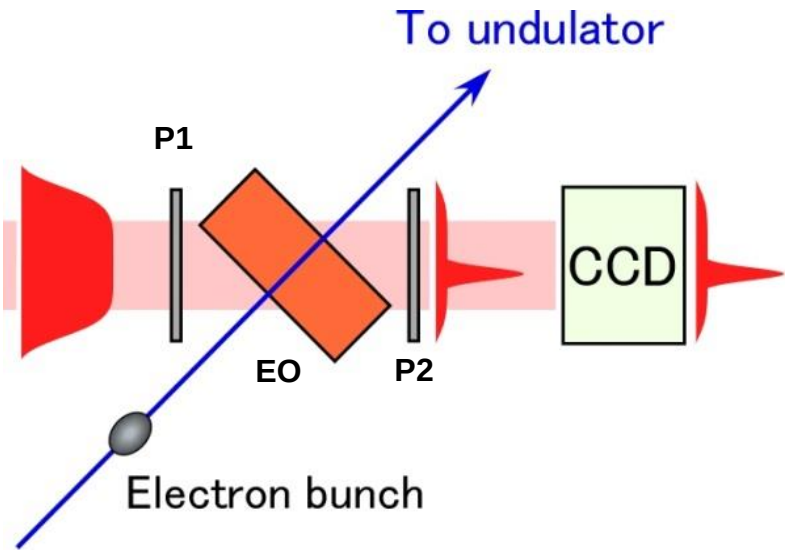

Figure 3. A schematic drawing of the spatially decoding EO sampling measurement.

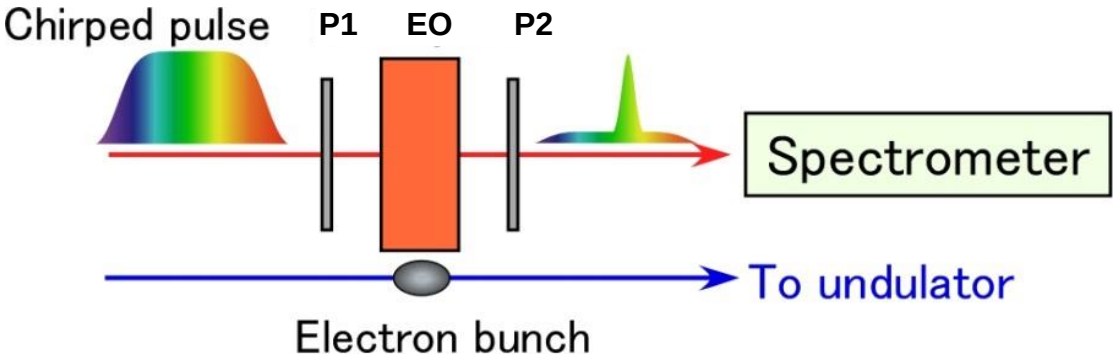

Figure 4. A schematic drawing of the spectrally decoding EO sampling method. A linearly chirped probe pulse passes through the polarizer P1 and the EO crystal. After transmitting the polarizer P2, the probe pulse is detected by a spectrometer. The phase retardation is converted into the spectral intensity moderation by the spectrometer. The polarizer P1 and P2 are put in crossed Nicol.

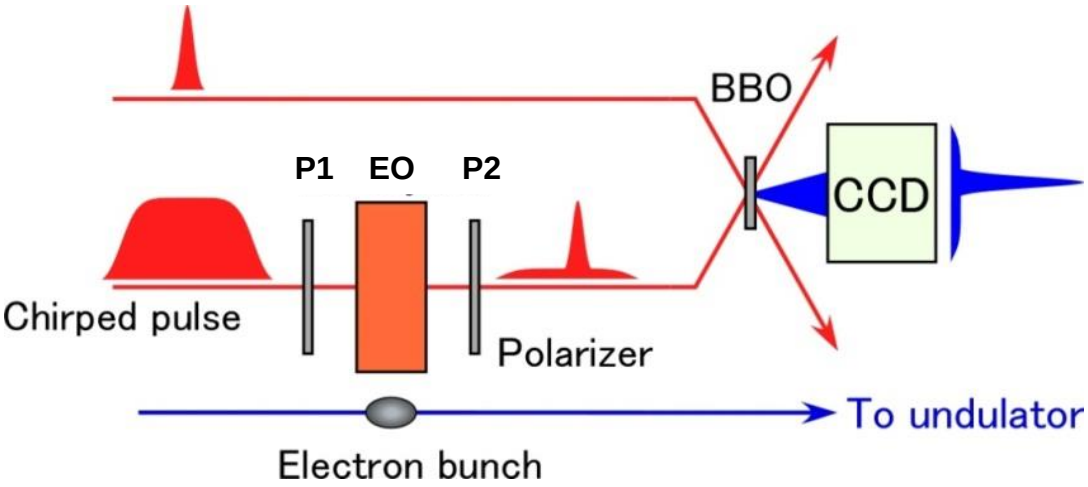

Figure 5. A schematic drawing of a temporally decoding EO sampling method. The probe pulse with a short temporal width is separated into two pulses. One is not stretched. The other is linearly chirped and passes through the polarizer P1 and EO crystal. After passing through the polarizer P2, the temporal profile of the chirped pulse represents the temporal structure of the electron bunch. The temporal profile of the chirped pulse is detected by the single shot cross correlation method.

2. Experiments

2.1. SCSS test accelerator

In this experiment, the SPring-8 Compact SASE Source (SCSS) test accelerator [23] at the RIKEN Harima Branch was used. The SCSS test accelerator consists of four sections: the low emittance injector, the magnetic chicane based bunch compressor, the C-band linear accelerator and two undulators in a vacuum [24]. A schematic drawing of the SCSS test accelerator is shown in Fig. 6.

The hot cathode made of a single crystal CeB_6 heated up to 1800 K is used in a 500 keV electron gun [25]. The gun emits electron beams with a temporal width of 2 μs and a peak current of 1 A. The high-voltage pulsed beam deflector slices an electron bunch with the temporal width of 600 fs from the electron beam. The fluctuation of the high-voltage of the deflector causes the fluctuation of the temporal bunch width. In this thesis, the charge amount of the sliced electron bunch was 0.4 nC/bunch. The S-band (2856 MHz) accelerator increases the energy of the electron bunch up to 45 MeV. Then the following C-band (5712 MHz) linear accelerator increases the energy up to 250 MeV. The dark current from the C-band accelerator system is removed by the following magnetic chicane. The electron bunch is injected into two undulators.

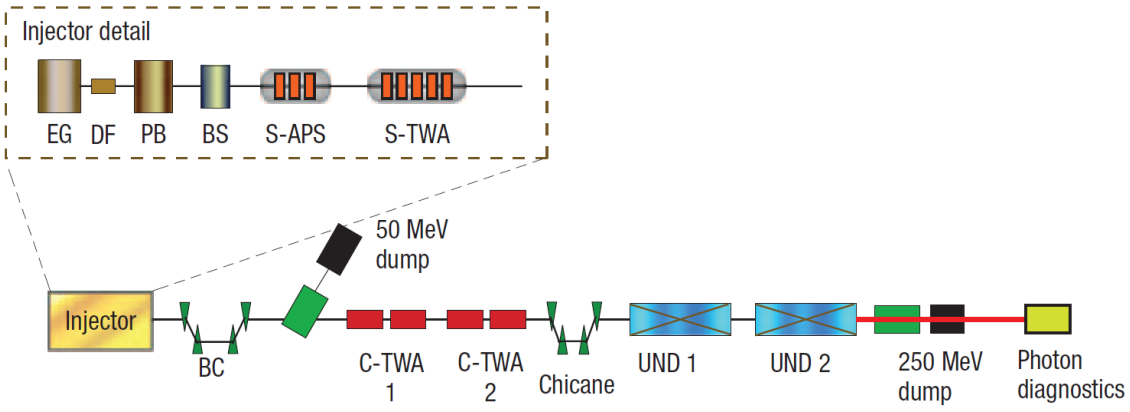

Figure 6. A schematic drawing of the SCSS test accelerator [23].

Each undulator has 300 periods of permanent magnets, and the length of the period is 15 mm. Pairs of steering magnets are installed at the entrance and the exit of the two undulators to optimize the electron trajectory. The radiation wavelength can be tuned by changing the undulator parameter K, and K is adjustable by changing the length of the undulator gap.

2.2. Synchronized Ti:Sapphire laser system

A home-built Ti:Sapphire laser was used for the generation of 13th and 15th order harmonics and the probe laser for the EO sampling measurement. The Ti:Sapphire laser system was composed of the oscillator (Tsunami, Spectra Physics), which was synchronized to the clock of the accelerator, the regenerative amplifier (Spitfire, Spectra Physics), and the 4-pass amplifier. The central wavelength of the output pulse was 800 nm, the bandwidth was 8 nm, temporal width was 150 fs, and the pulse energy was 30 mJ/pulse. An acoustic-optic programmable dispersive filter (AOPDF) (Dazzler, FASTLIGHT) was placed after the oscillator, and the generation of the high order harmonics was optimized by compensating for the second and the third order dispersion by using Dazzler.

Since the interval of each pulse generated in the oscillator is $2L/c$, where L is the length of the oscillator and c is the speed of light, Ti:Sapphire laser is synchronized to the clock of the accelerator by adjusting L. A schematic of the synchronization is shown in Fig. 7. The oscillator was synchronized to the 79.3 MHz signal which was divided from the 238 MHz radio frequency (RF) signal for the accelerator. The RF signal was synchronized to the AC 60 Hz for the stable operation of the electric devices, such as the electron gun and the deflector. The timing of the pockels-cell of the regen-

erative amplifier and the pump laser for the 4-pass amplifier was synchronized to the 30 Hz trigger signal for the FEL.

2.3. High order harmonic generation

The output of the Ti:Sapphire laser was loosely focused into the Xe gas cell by a f = 4 m lens. Loosely focused femtosecond laser pulses with a phase matching condition can generate intense high order harmonic pulses [7, 8]. The pressure of the Xe gas cell was tuned to optimize the energy of the 13th or 15th order harmonic pulse, and the pressure was about 53 Pa. The fundamental pulses and the 13th order harmonics were separated by two harmonic separator mirrors coated with Si with the Brewster angle (75 degrees) for the P polarized beam at λ = 800 nm [9]. To accomplish the seeding of the FEL by an external laser, the intensity of the seeding laser should be larger than the spontaneous radiation emitted at the entrance of the first undulator [27]. The separated 13th order harmonic pulses were collimated and focused by two concave mirrors coated by Pt to surpass the spontaneous radiation intensity at the entrance of the first undulator. The pulse energy of the 13th order harmonic pulse at the entrance of the undulator was about 2 nJ, and the temporal pulse width was estimated to be 50 fs [10]. The spectrum of the 13th order harmonics is shown in Fig. 9.

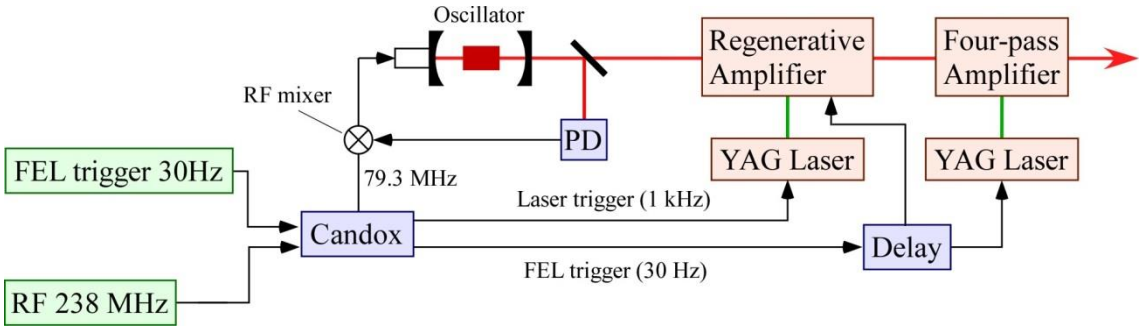

Figure 7. The timing system of the Ti:Sapphire laser.

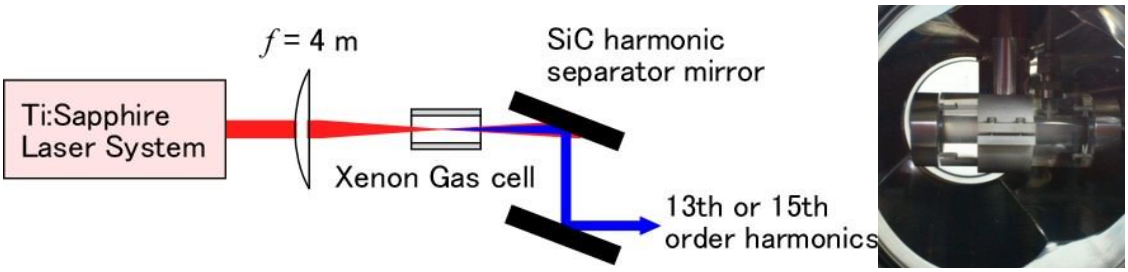

Figure 8. A schematic picture of the generation of the 13th and 15th order harmonics (left), and the photo of the Xe gas cell (right). Two harmonic separator mirrors were put at a 75 degree angle, which was the Brewster angle for a P polarized beam at λ = 800 nm. The pulse energy of the fundamental pulse after the harmonic separators was less than 0.25 % of the incident pulse energy.

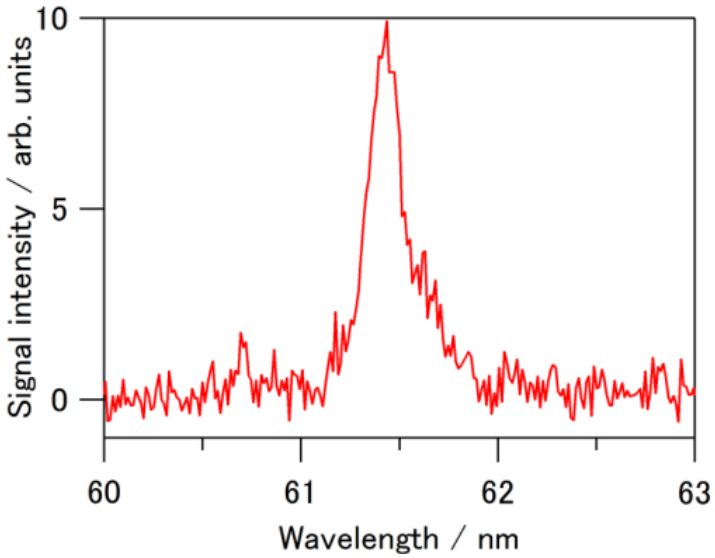

Figure 9. The spectrum of the 13th order harmonic pulse. The spectral bandwidth was 0.5 nm, and the Fourier transform limited pulse width was 46 fs.

2.4. Measurement of the arrival time

OTR method

The arrival time between the electron bunch and the Ti:Sapphire laser was measured by using the optical transition radiation (OTR) emitted from the electron bunch and the streak camera (FESCA-200, Hamamatsu Photonics K.K.).

The transition radiation is emitted at the boundary of two media with different dielectric constants when a charged particle passes through the boundary. The transition radiation is explained by the change of the dipole moment induced in both media around the boundary. The radiation is emitted in both the forward and the backward directions of the boundary. When the wavelength of the radiation is in the visible wavelength region (400 nm < λ < 800 nm), the radiation is called an optical transition radiation. The maximum energy of the transition radiation is emitted at an angle which is the inverse of the relativistic Lorentz factor γ. The OTR is used to measure the longitudinal charge distribution of the electron bunch [28] and the arrival time of the electron bunch. In this research the OTR and the Ti:Sapphire laser pulse were detected by the streak camera and used to measure the arrival time of the electron bunch and the Ti:Sapphire laser pulse. The image of the streak camera when the arrival timing of the Ti:Sapphire laser was earlier than that of the FEL by 10 ps was shown in Fig. 10.

This method is a destructive measurement because the high-order harmonic pulse is intercepted to introduce the undulator by the OTR screen. This means the arrival time cannot be measured during the seeding of the FEL. In this experiment, the arrival time varied by about 10 ps per an hour as shown in Fig. 1. Since this arrival time drift is larger than the temporal width of the electron bunch and the 13th order harmonic pulse by more than a first-order magnitude, the temporal overlap cannot be

kept for a long time. The arrival time should be monitored and the arrival time drift should be compensated in real time in order to keep the temporal overlap for a long time. The arrival time monitor based on the EO sampling technique was introduced in this thesis.

EO sampling method

The transmittance of the high reflective mirror for 800 nm which was located at the optical pass for the high order harmonic generation was used as a probe laser for the spectrally decoding EO sampling measurement. The probe pulse was linearly chirped by the high dispersive glass rods and AOPDF (Dazzler, FASTLIGHT) up to 10 ps. The photograph of optical layout and a schematic drawing of the EO sampling measurement are shown in Fig. 12 and Fig. 13. The first order diffraction from the Dazzler was introduced into the vacuum chamber. A ZnTe crystal cut by the (110) plane whose thickness was 1 mm was put in the vacuum chamber. A picture of the ZnTe crystal and the Ce^{3+} doped yttrium aluminum garnet (Ce:YAG) crystal is shown in Fig. 14. The Ce:YAG crystal was used to detect the position of the those crystals, because Ce:YAG emits strong and long-lived fluorescence when the electron bunch travels through the Ce:YAG crystal. The distance between the ZnTe crystal and the trajectory of the electron bunch was about 2 mm. Two polarizers were placed before and after the ZnTe crystal and they put in crossed-Nicol. The phase retardation was converted into a spectral modulation after the second polarizer, and the spectral modulation was detected by the spectrometer (QE65000, Ocean Optics).

The spectrum of the probe pulse averaged for 300 shots when the electron bunch did not pass by the EO crystal was used as a background spectrum. The back-

ground spectrum was subtracted from the detected EO signal. The spectrum of the EO signal and the background signal is shown in Fig. 11. A home-built LabView program was used to record the EO signal and the central wavelength of the EO signal. In this research, the pulse with a 150 fs temporal width was stretched up to 10 ps, and the temporal resolution of the spectrally decoding EO sampling measurement was about 1.3 ps.

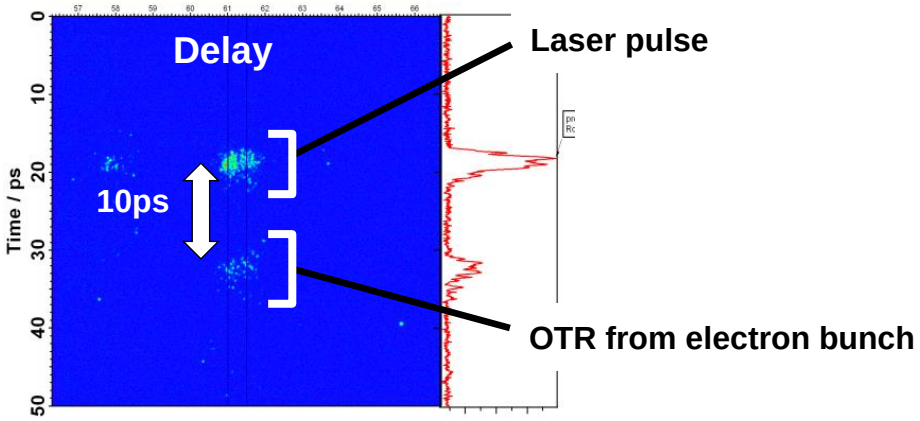

Figure 10. The streak image when the timing of the Ti:Sapphire laser was earlier than the timing of the electron bunch by 10 ps.

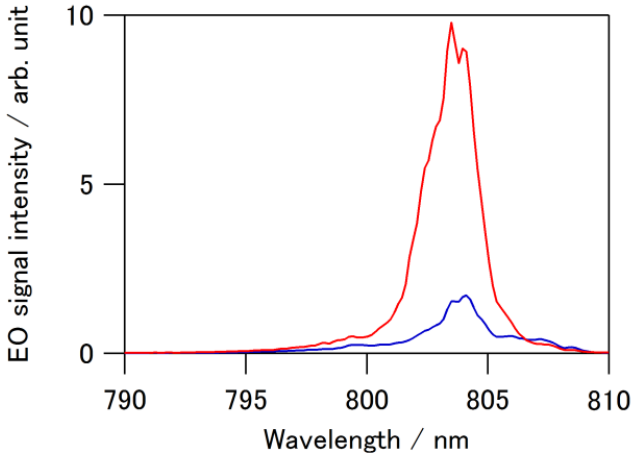

Figure 11. A single shot spectrum of the probe pulse after the EO crystal and the crossed-Nicol polarizer. The red line: the spectrum when the electron bunch passed by the EO crystal. The blue line: the spectrum when the electron bunch did not pass by the EO crystal, namely the background spectrum.

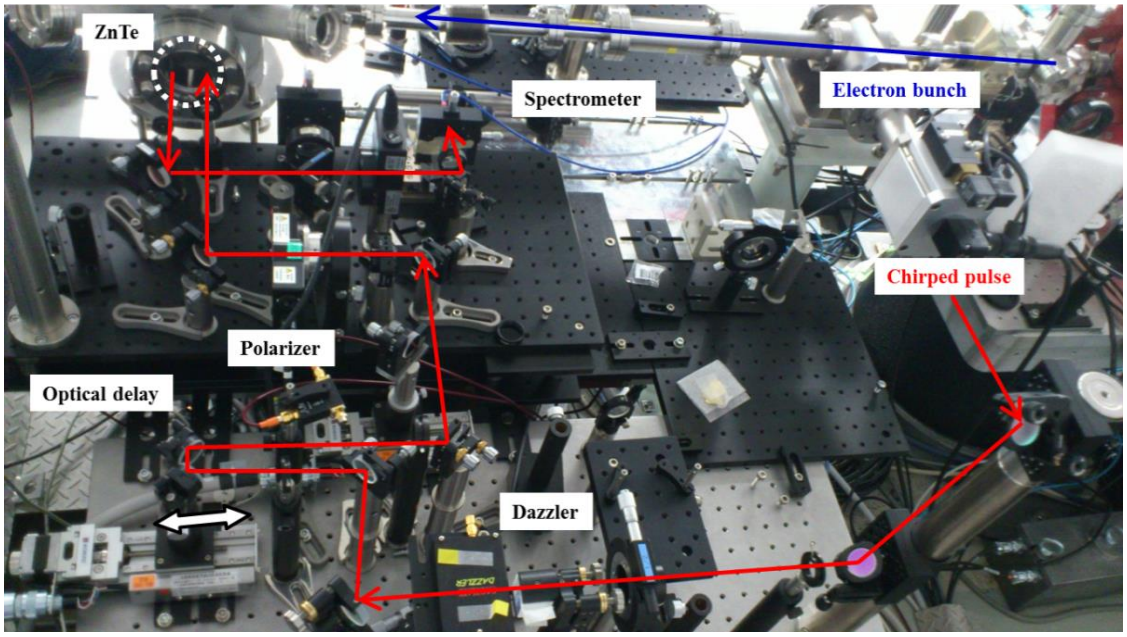

Figure 12. The optical layout of the EO sampling measurement. The blue arrow shows the trajectory of the electron bunch. The red arrow shows the optical pass of the probe pulse. A ZnTe crystal was put in the vacuum chamber (white dashed circle). The EO signal was detected by a fiber spectrometer.

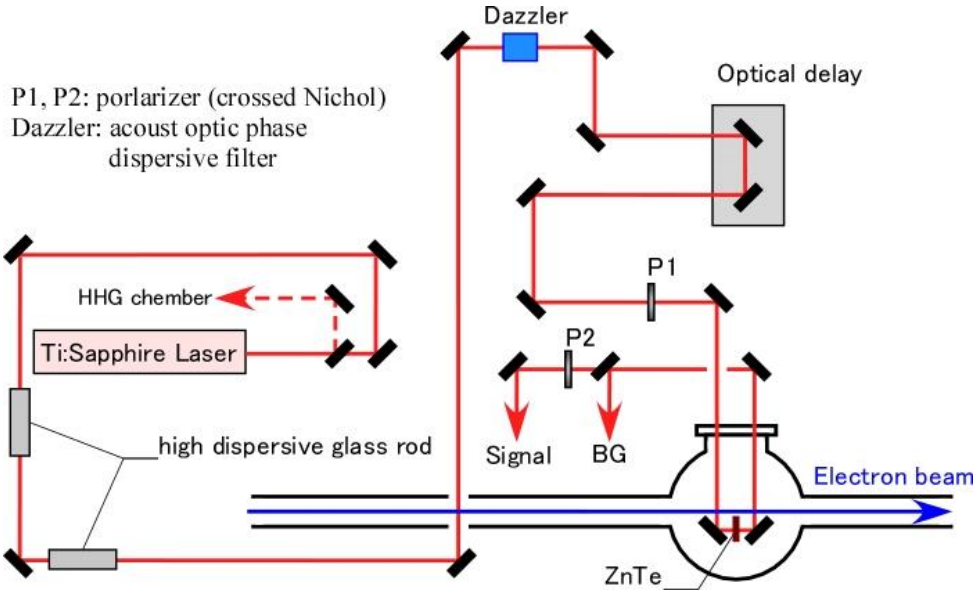

Figure 13. A schematic drawing of the spectrally decoding EO sampling measurement. A linear chirp was added to the probe pulse by high dispersive glass rods and the Dazzler. The ZnTe crystal was put 2 mm away from the trajectory of the electron beam.

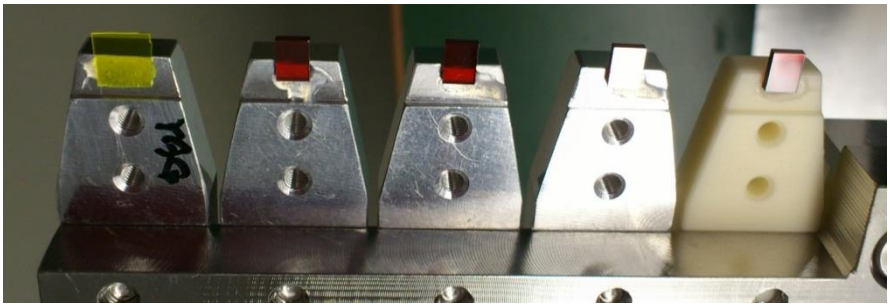

Figure 14. The first to the fourth from the right are the ZnTe crystals used in this thesis. The crystals were cut in the (110) plane and their thickness was 1 mm. The one on the right end was mounted on a holder made of ceramic. The current would flow in the metallic holder, and the birefringence in the ZnTe crystal would be affected by the current. The ceramic holder was prepared for such an effect. In this thesis, there were no significant differences between the metallic holder and the ceramic holder. The crystal on the left end was a Ce:YAG. When the electron bunch hit the Ce:YAG, the strong fluorescence was emitted from the crystal. The Ce:YAG was used to check the position of the crystals.

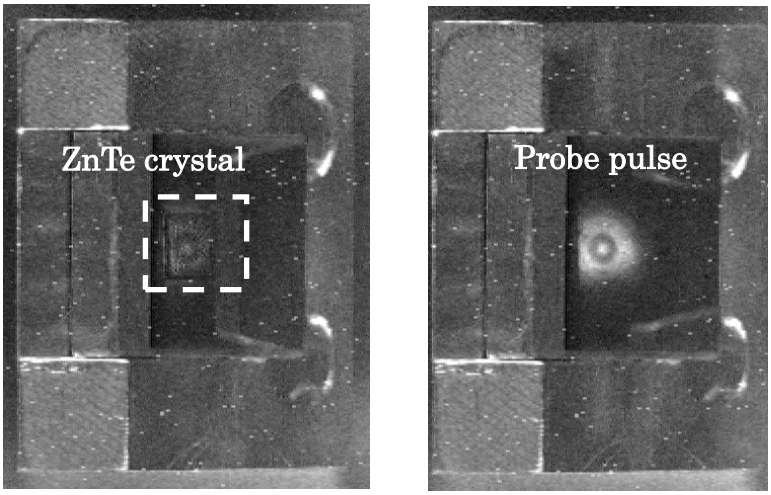

Figure 15. The CCD image of the ZnTe crystal in the vacuum chamber. It was confirmed that the probe pulse hit the ZnTe crystal correctly.

2.5. Control of the timing of Ti:Sapphire laser

A high-precision trigger and clock delay module (84DgR5CO1, Candox Systems) which can change the delay of the RF signal with a high accuracy was used to adjust the trigger delay of the Ti:Sapphire laser with a resolution of 200 fs. The delay module tunes the delay time by changing the phase of the RF signal. If the initial frequency of the RF is f and the initial phase is φ_0, the RF signal can described as

$$I(t) = \sin(2\pi ft + \varphi_0). \quad (4)$$

If the delay time τ is added to the RF signal,

$$I(t-\tau) = \sin(2\pi f(t-\tau) + \varphi_0)$$
$$= \sin\left(2\pi ft + (\varphi_0 - 2\pi f\tau)\right). \quad (5)$$

Eq. (4) corresponds to the initial phase shit by $-2\pi f\tau$. The synchronization timing was tuned in real-time to keep the pulse energy of the amplified EUV pulses and the central wavelength of the EO signal constant by tuning the delay time of the delay module.

2.6. Gas monitor detector

A gas monitor detector developed by DESY, PTB and Ioffe [29, 30] was used to measure the energy of the FEL pulses at the SCSS test accelerator [31]. The detector is based on the one photon ionization of argon. The detector consisted of a vacuum chamber equipped with a differential pumping system and filled with 10^{-2} Pa of Ar. The Ar^+ and the electron derived from the one photon single ionization of Ar were detected by Faraday cups. The detected current was amplified and converted into a digital signal. The digital signal was saved on Ayagiku, which is the database of the SCSS test accelerator in micro joule unit. The unit conversion from current to joule was calibrated by the gas monitor detector used in DESY at 51.3 nm, 56.1 nm, and 61.2 nm [30].

The gas monitor detector was located after the two steering mirrors coated with SiC as shown in Fig. 17. The gas monitor detector measures the pulse energy reduced by the reflectivity of the SiC mirror. The incident angle of the two steering mirrors was 85 degrees, and the reflectivity of the P polarized pulse at the incident angle of 85 degrees was calculated by Fresnel's equation. The reflectivity of SiC at λ = 61.5 nm was obtained to be 0.89. The pulse energy just behind the second undulator was 1.27 times larger than the pulse energy measured by the gas monitor detector.

2.7. The overlap between the electron bunch and the seeding laser

The spectral overlap

The wavelength of the undulator radiation was matched to the wavelength of the 13th or 15th order harmonics by tuning the undulator gap. Fig. 16 shows the spectrum of the undulator radiation and the 13th order harmonics.

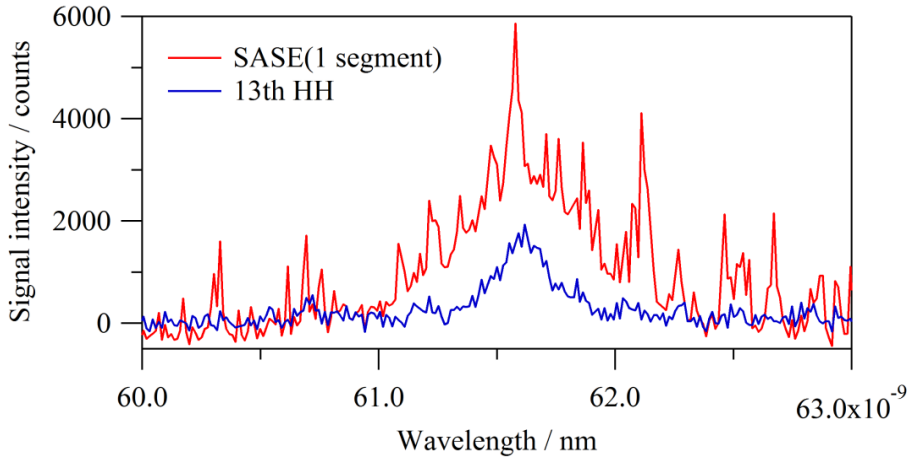

Figure 16. The spectrum of the 13th order harmonics of λ = 800 nm (blue line), and the undulator radiation (red line). The wavelength of the undulator radiation was optimized by adjusting the undulator gap.

The spatial overlap

A thin film made of Au and a phosphor screen equipped with a micro channel plate was used to detect the position of the high order harmonics and the OTR emitted from the electron bunch. The spatial position was monitored before and after the first undulator by using a micro channel plate equipped with a phosphor screen and a CCD camera. The position of the high-order harmonic pulses was adjusted by tuning the Pt concave mirrors, which were used to collimate and to focus the high-order harmonics.

The temporal overlap

First, the trigger delay of the Ti:Sapphire laser was adjusted to amplify the 13th order harmonics. Second, the optical delay and the first order dispersion of the Dazzler introduced into the optical setup to monitor the arrival time as shown in Fig. 12 and Fig. 13 was tuned to detect the EO signal at the moment when the 13th order harmonics were amplified. The trigger delay of the Ti:Sapphire laser was tuned to keep the central wavelength of the EO crystal and the energy of the EUV pulses constant.

A schematic drawing of the whole experimental setup is shown in Fig. 17. Ti:Sapphire laser pulses were focused into the Xe gas cell to generate 13th and 15th order harmonic pulses. The Pt concave mirrors were used to focus the high-order harmonic pulses and to overlap the high-order harmonic pulses with the electron bunches. The arrival time between the electron bunch and the Ti:Sapphire laser pulse was monitored just before the first undulator. The spectrum of the FEL pulses was detected by the EUV spectrometer located after the second undulator. The pulse energy was measured by the gas monitor detector.

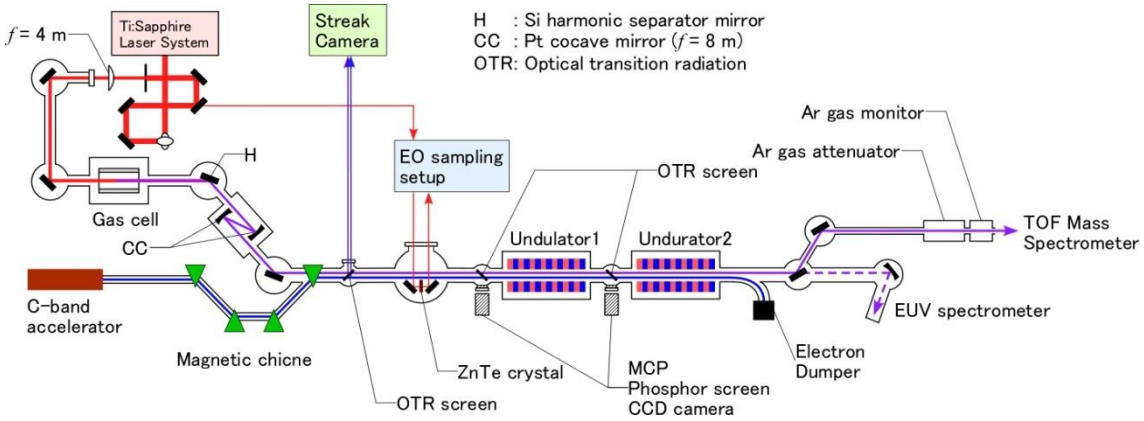

Figure 17. The experimental setup for the free-electron laser seeded with the 13th and the 15th order harmonics of Ti:Sapphire laser.

3. Results and Discussion

3.1. The arrival time measurement and the timing drift compensation

The single-shot and the averaged change of the peak wavelengths of the EO signal are shown in Fig. 18.

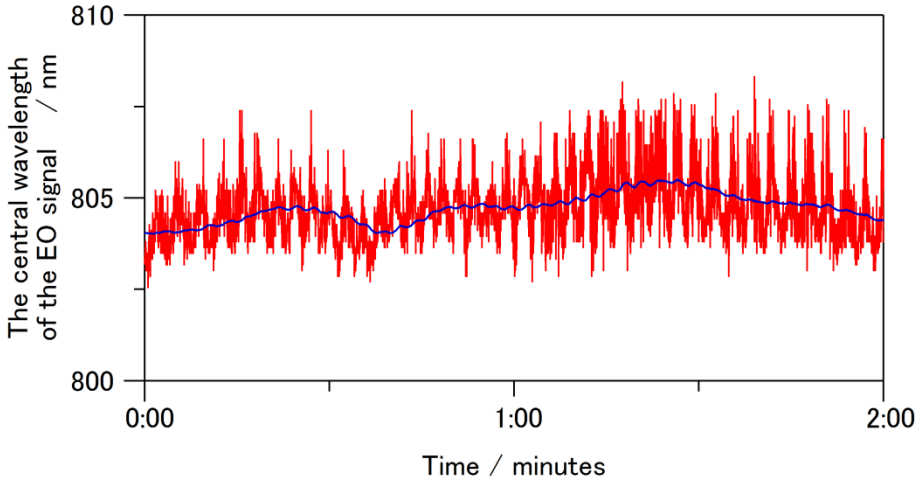

Figure 18. The central wavelength of the EO signal. Red line: the central wavelength of the single shot EO signal. Blue line: the central wavelength of the averaged EO signal for 100 shots.

Since the probe pulse was lineally chirped in the spectrally decoding EO sampling measurement, the relationship between the arrival time and the central wavelength of the EO signal is:

[The arrival time (fs)] = [The central wavelength of the EO signal (nm)]

× [The chirp rate of the probe pulse (ps/nm)]

In this thesis, the chirp rate was measured by changing the trigger delay of the Ti:Sapphire laser by using Candox. The change of the central wavelength of the EO signal when the timing of the Ti:Sapphire laser was adjusted was shown in Fig. 19. A 1 ps trigger delay change corresponded to a 1.2 nm central wavelength shift in the EO signal. The chirp rate was obtained as 0.8 ps/nm. To measure the chirp rate more accurately, a cross correlation of the probe pulse should be measured. The trigger delay time shown in Fig. 20(a) was added to the trigger delay module for two hours. As a consequence, the jitter and the drift were suppressed to less than 1 ps, as shown in Fig. 20(b). If the trigger delay had not been adjusted, the arrival time drift which corresponds to the delay time shown in Fig. 20(a) would have been observed.

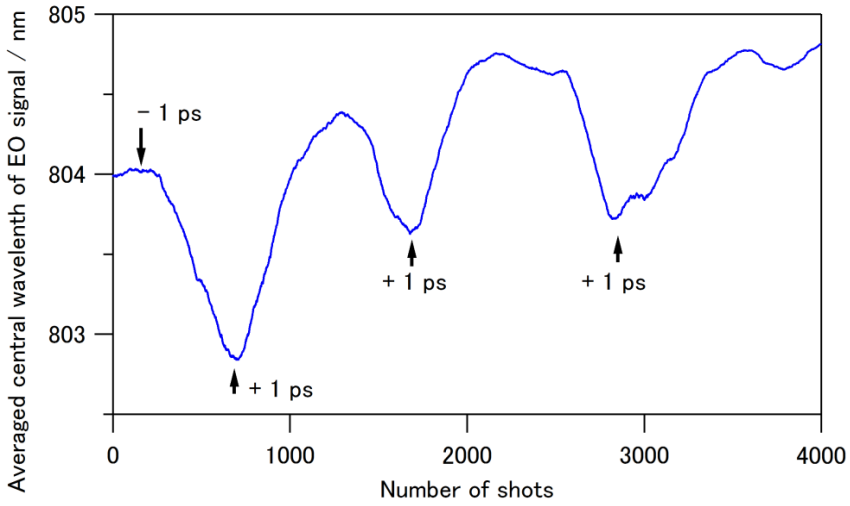

Figure 19. Changes in the central wavelength of the EO signal when the trigger delay time was changed by using Candox. The arrows show the points at which the trigger delay was changed.

3.2. Spectrum of the FEL pulse seeded by 13th order harmonics

Figure 21 shows the single shot spectrum of the FEL pulse seeded by the 13th order harmonics of λ = 800 nm and the SASE-FEL pulse under the same condition of the electron bunch and the undulator. The improvement of the spectrum coherence was confirmed for the FEL seeded by the 13th order harmonics. The spike-like structure was confirmed at the edge of the spectrum. The temporal width of the 13th order harmonics was about 50 fs, which was less than one over ten of the temporal width of the electron bunch. The small spectral moderation was derived from the SASE-FEL radiated from the electron bunch which was not overlapped with the 13th order harmonics.

The spectra of the seeded FEL pulses of 8 shots which had more than 5 arbitrarily units of peak intensity is shown in Fig. 22. The central wavelength of the seeded FEL pulse was 61.4(1) nm, and the spectral bandwidth was 0.11(2) nm. The corresponding Fourier transform limited pulse duration was 46(6) fs. The temporal width of the 13th order harmonics was estimated to be about 50 fs [20]. The temporal width of the seeded FEL pulse was almost the same as the temporal width of the 13th order harmonics.

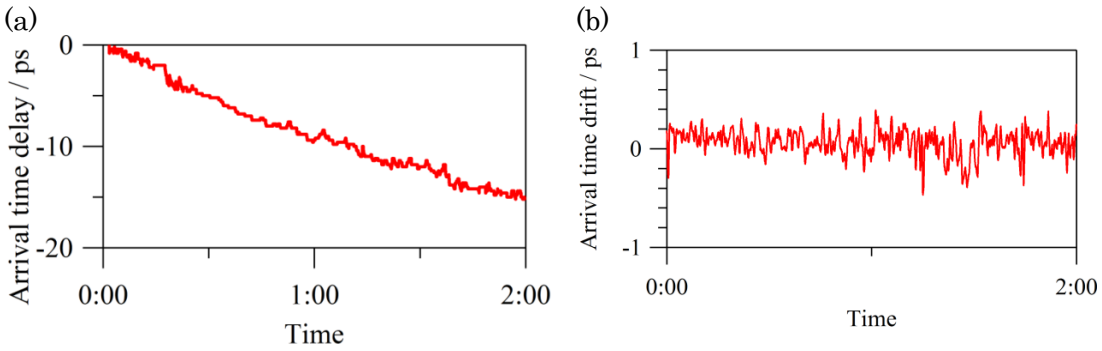

Figure 20. (a) The trigger delay time added to the Candox by using the home-built LabView program. (b) The arrival time of the electron bunch when the trigger delay was adjusted.

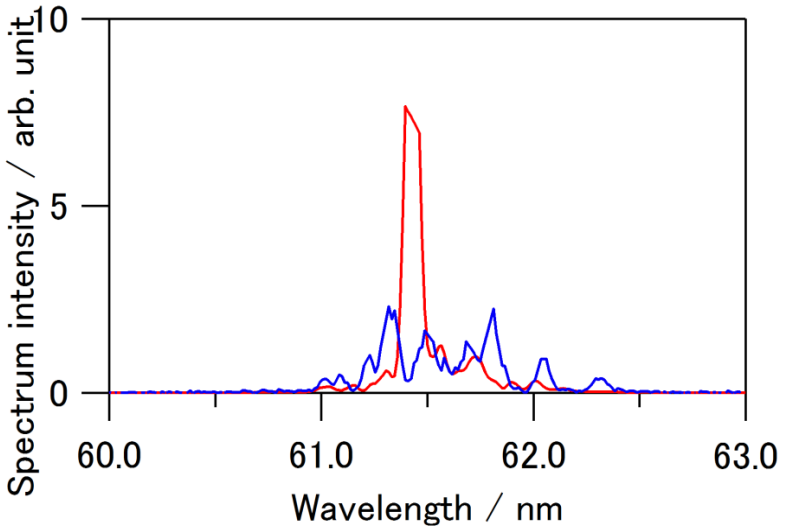

Figure 21. The single shot spectrum of the SASE-FEL pulse (blue line), and the FEL pulse seeded by 13th order harmonics (red line). The small spectral moderation of the seeded FEL pulses was derived from the SASE-FEL.

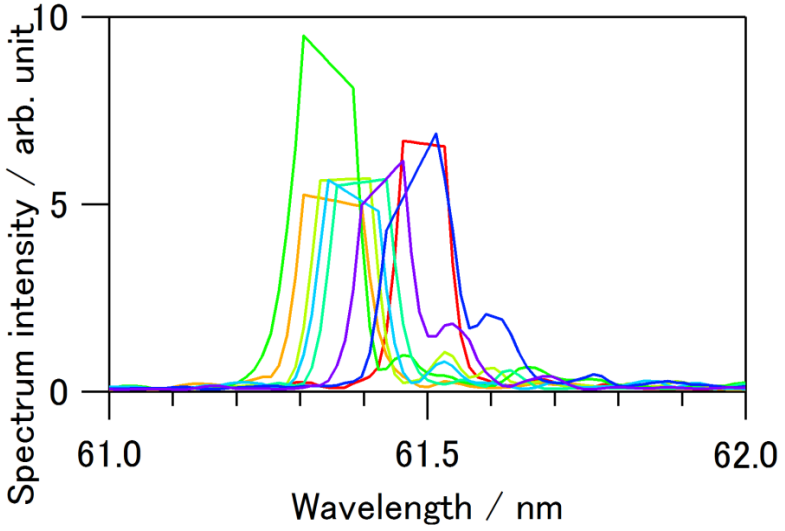

Figure 22. The single shot spectra of the seeded FEL pulses.

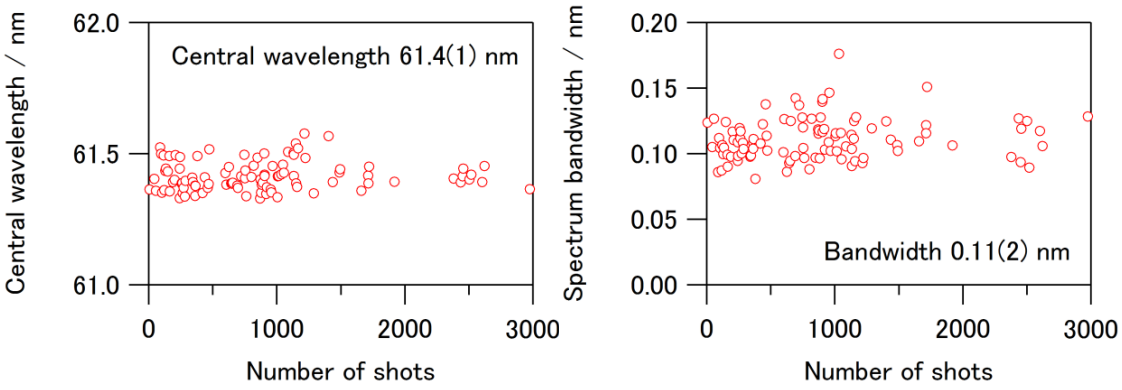

Figure 23. The central wavelength (left) and the bandwidth (right) of the seeded FEL pulse. Pulses which had more than 5 arbitrarily units of spectral peak intensity was picked up in this figure.

3.3. Pulse energy of the FEL pulses seeded by the 13th order harmonics

The single shot pulse energy of the FEL with and without the introduction of the 13th order harmonics is shown in Fig. 24. The histogram of the each pulse energy is shown in Fig. 25. The pulse energy of the FEL pulses without the 13th order harmonics was less than 2μJ. The FEL pulses which have more than 2 μJ per pulse are seeded by the 13th order harmonics. The ratio of the number of the seeded FEL pulses with respect to the total number of shots was more than 15 %, which was larger by two orders of magnitude than in the previous study [20]. This improvement is thought to be due to the improvement of the temporal overlap between the electron bunch and the 13th order harmonics. The pulse energy of the seeded FEL pulse shown in Fig. 25 fluctuated shot by shot. This fluctuation mainly originated from the fact that the pulse energy of the seeded FEL pulse did not achieve the saturation regime. The fluctuation of the maximum pulse energy shown in Fig. 24 also supports that the seeded FEL pulse did not achieve the saturation regime.

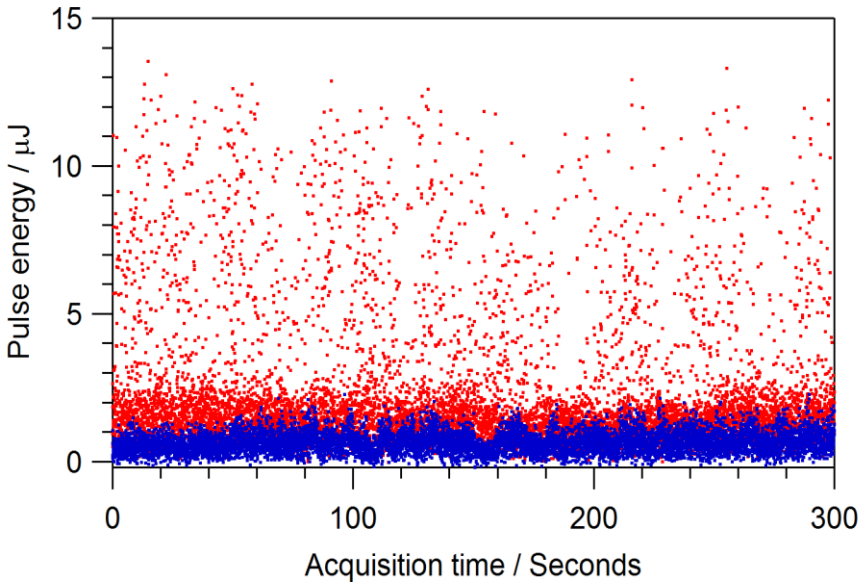

Figure 24. The single shot pulse energy of the FEL pulse. Red dots: the FEL pulse energy when the 13th order harmonics seeding was introduced. Blue dots: the FEL pulse energy when the 13th order harmonics seeding was not introduced. The energy fluctuation signifies that the FEL pulse energy did not achieve the saturation regime.

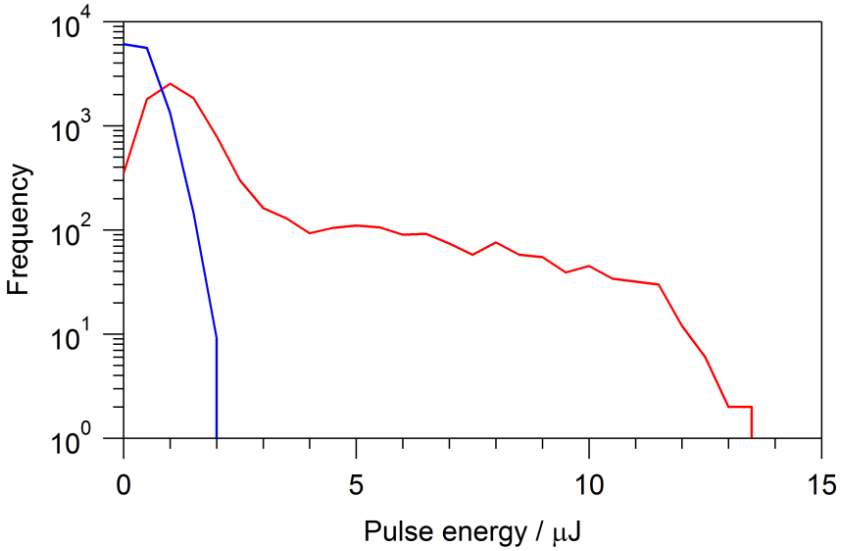

Figure 25. The histogram of the single shot FEL pulse energy shown in Fig. 24. The red line: The FEL pulse energy when the 13th order harmonics seeding was introduced. The Blue line: The FEL pulse energy when the 13th order harmonics seeding was not introduced. Since the FEL pulse energy when the seeding pulse was not introduced was less than 2 μJ, the FEL pulse with the energy of more than 2 μJ per pulse was seeded by the 13th order harmonic pulses.

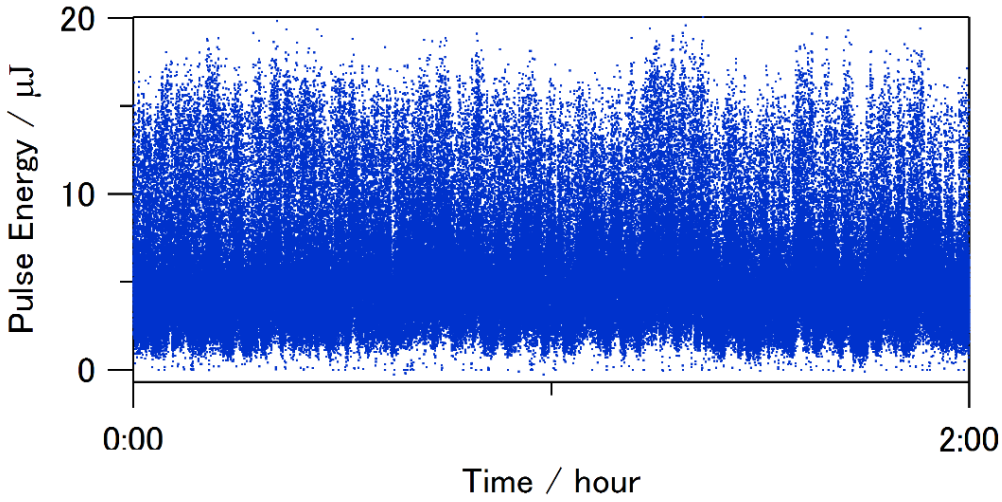

Figure 26. The single shot pulse energy of the FEL when the seeding by 13th order harmonic pulses was introduced into the undulators. The large energy fluctuation signifies that the FEL saturation regime was not accomplished. Since the arrival timing drift was compensated, the FEL was seeded by the 13th order harmonic pulses for a long time.

Figure 26 shows the FEL pulse energy when the 13th order harmonic pulses were introduced into the undulator with the electron bunch. Since the arrival time drift was suppressed to less than 1 ps, which is shown in Fig. 20(b), the seeded FEL pulses were generated for long time. This means that it is possible to use the seeded FEL pulses as a light source for the experiments, such as in observing the multiphoton ionization by using the time-of-flight mass spectrometry.

3.4. Second order harmonic generation of 61.5 nm

The generation of the second harmonic of the amplified 13th-order harmonic was confirmed at λ = 30.7 nm. The spectrum of the second harmonic was shown in Fig. 27. The second harmonic should be the seed pulse to generate the coherent pulses in the Soft X-ray or shorter wavelength region, because it is difficult to generate high-order harmonics of Ti:Sapphire laser pulses which are intense enough to seed the FELs.

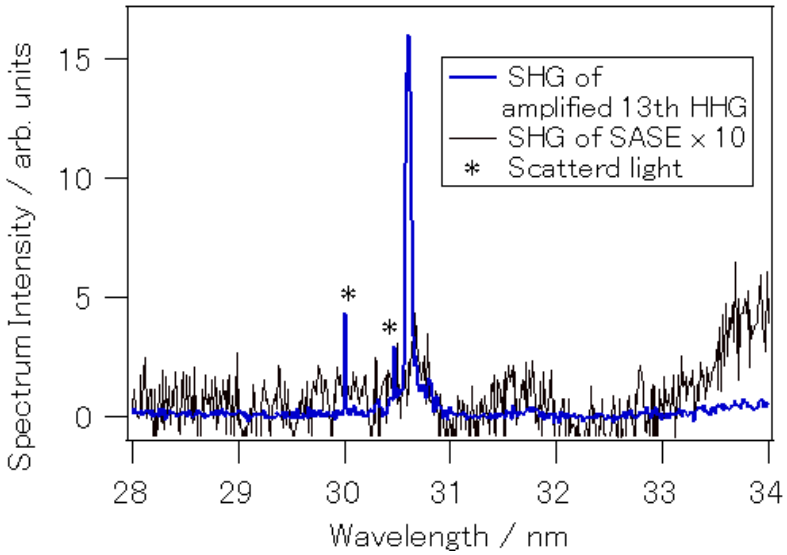

Figure 27. The spectrum of the second harmonics of 61.5 nm. A significant amplification with respect to the SASE-FEL was confirmed.

4. Conclusion

The FEL was seeded by the 13th and 15th order harmonics of Ti:Sapphire laser to increase the peak power of the FEL pulses and to generate a strong field in the EUV wavelength region. The spectrum of the seeded FEL pulses was a single-peak structure and the pulse energy was up to 20 μJ. The pulse energy of the seeded FEL pulses fluctuated shot by shot, and this fluctuation was thought to be due to the fact that the seeded FEL pulses did not achieve the saturation regime. The important condition to generate the FEL seeded by the high-order harmonics is the temporal, spatial, and spectral overlap between the electron bunch and the high-order harmonics. Although the arrival timing drift between the electron bunch and the Ti:Sapphire laser pulse was within 1 ps for 20 to 30 seconds, it was difficult to seed the FEL by 13th and 15th order harmonics for a long time. This was an obstacle for applying the seeded FEL pulses to our application experiments. The arrival time monitor based on the spectrally decoding EO sampling scheme enabled us to monitor the arrival time non-destructively in real

time. The trigger delay time of the Ti:Sapphire laser was adjusted by the home-built LabView program. As a consequence, the arrival time drift was compensated with sub-ps accuracy, and the FEL was seeded by the high-order harmonics for long time. The generation of the second harmonic of the amplified 13th-order harmonic shows that the combination of the external seeding scheme and the high gain harmonic generation scheme would be one of the coherent light sources in the Soft X-ray and shorter wave-length regions.

Appendix

A. Optical transition radiation

The radiation energy *U* emitted to the backward direction when a single electron with a charge of -*e* passes through the boundary between vacuum to a metal is descried by the Ginzburg - Frank fomula

$$U = \int_0^{\infty} \int_0^{2\pi} \int_0^{\pi} d\omega d\phi \sin\theta d\theta \frac{e^2}{4\pi^3 \varepsilon_0 c} \frac{\beta^2 \sin^2\theta}{(1-\beta^2\cos^2\theta)^2}, \quad (5)$$

where $\beta = v/c$, and θ is the radiation angle.

The total radiation energy emitted from a metallic boundary is derived from the integration of the equation (6) over the solid angle $d\Omega = \sin\theta \, d\theta d\phi$.

$$\begin{aligned} \frac{dU}{d\omega} &= \int d\theta d\phi \sin\theta \frac{e^2}{4\pi^3 \varepsilon_0 c} \frac{\beta^2 \sin^2\theta}{(1-\beta^2\cos^2\theta)^2} \\ &= \frac{e^2\beta^2}{2\pi^2 \varepsilon_0 c} \int d\theta \frac{\sin^2\theta}{(1-\beta^2\cos^2\theta)^2}, \\ &= \frac{e^2}{8\pi^2 \varepsilon_0 c} \left(4 + \frac{(1+\beta^2)}{\beta} \log \frac{(1-\beta)^2}{(1+\beta)^2}\right), \end{aligned} \quad (6)$$

The angler distribution can be obtained from the differentiation of the Ginzburg-Frank formula with respect to the radiation angle θ.

$$\frac{dU}{d\theta} = \frac{\rho_{q,\omega}}{4\pi^3} \frac{\beta^4 c \sin 2\theta}{(1-\beta^2\cos^2\theta)^3} \{1 - \beta^2 - \beta^2 \sin^2\theta\}, \quad (7)$$

The radiation energy becomes maximum when the equation (7) is zero. When the angle that the radiation energy becomes maximum is small, the angle is represent as the equation (8).

$$\theta_{max} = \sin^{-1} \frac{1-\beta^2}{\beta^2} \approx \frac{1-\beta^2}{\beta^2}, \quad (8)$$

B. Electro-Optic effect in a birefringence crystal

The index ellipsoid

The relationship between the electric field and the first order polarization in an anisotropic medium is described as the following equation (9).

$$\boldsymbol{P} = \varepsilon_0 \chi_{jk}^{(1)} \boldsymbol{E}\,, \tag{9}$$

where $\chi_{jk}^{(1)}$ is the first order susceptibility tensor. The first order susceptibility tensor depends on the coordinate system of the crystal. The orthogonal axes of the coordinate system in which the tensor is diagonal are called the principal axes of the crystal.

The electric displacement vector $\boldsymbol{D}$ is described as equation (2.2),

$$\boldsymbol{D} = \varepsilon_0 \boldsymbol{E} + \boldsymbol{P} = \varepsilon_0 \varepsilon \boldsymbol{E}\,, \tag{10}$$

where $\boldsymbol{E}$ is electric field, ε_0 is dielectric constant of vacuum, ε is the relative permittivity of medium.

In the *xyz* coordinate system where the *x*, *y*, and *z* axes are the principal axes of the crystal, equation (10) becomes

$$\boldsymbol{D} = \begin{pmatrix} \varepsilon_x & 0 & 0 \\ 0 & \varepsilon_y & 0 \\ 0 & 0 & \varepsilon_z \end{pmatrix} \begin{pmatrix} E_x \\ E_y \\ E_z \end{pmatrix}, \tag{11}$$

The energy density of the laser electric field is described as the equation (12).

$$U_e = \frac{1}{2} \boldsymbol{E} \cdot \boldsymbol{D} = \frac{1}{2} \sum_{i,j} E_i \varepsilon_{ij} E_j\,, \tag{12}$$

In the *xyz* coordinate system equation (12) is replaced by the eq. (13)

$$D_x{}^2/\varepsilon_x + D_y{}^2/\varepsilon_y + D_z{}^2/\varepsilon_z = 2U_e \tag{13}$$

By defining a vector $\boldsymbol{r}$ described as the eq. (14), the eq. (13) is replaced by the eq. (15). The principal indices of refraction are defined as the eq. (15).

$$\boldsymbol{r} = \begin{pmatrix} x \\ y \\ z \end{pmatrix} = \boldsymbol{D}/\sqrt{U_e}\,, \tag{14}$$

$$x^2/n_x{}^2 + y^2/n_y{}^2 + z^2/n_z{}^2 = 1\,, \tag{15}$$

The eq. (15) is called an index ellipsoid of a biaxial crystal. The major axes of the ellipsoid are parallel to the *x*, *y*, and *z* axes of the crystal, and those lengths represent refractive indices of the major axes.

The linear electro-optic effects

An electric field is impressed to crystals such as ZnTe, a linear electro-optic (EO) effect is induced. The index ellipsoid of the EO crystal is described as the eq. (16)

$$a_1x^2 + a_2y^2 + a_3z^2 + a_4yz + a_5zx + a_6xy = 1\,, \tag{16}$$

When an electric field is not impressed to an EO crystal, the coefficient vector $\boldsymbol{a}$ is represented by the eq. (17).

$$\boldsymbol{a} = \begin{pmatrix} 1/{n_x}^2 \\ 1/{n_y}^2 \\ 1/{n_z}^2 \\ 0 \\ 0 \\ 0 \end{pmatrix} = \begin{pmatrix} 1/{n_0}^2 \\ 1/{n_0}^2 \\ 1/{n_0}^2 \\ 0 \\ 0 \\ 0 \end{pmatrix}, \tag{17}$$

When an electric field $\boldsymbol{E}$ is impressed to an EO crystal, the coefficient vector $\boldsymbol{a}$ is represented by the eq. (18).

$$\boldsymbol{a} = \begin{pmatrix} 1/{n_0}^2 \\ 1/{n_0}^2 \\ 1/{n_0}^2 \\ 0 \\ 0 \\ 0 \end{pmatrix} + \begin{pmatrix} r_{11} & r_{12} & r_{13} \\ r_{21} & r_{22} & r_{23} \\ r_{31} & r_{32} & r_{33} \\ r_{41} & r_{42} & r_{43} \\ r_{51} & r_{52} & r_{53} \\ r_{61} & r_{62} & r_{63} \end{pmatrix} \begin{pmatrix} E_1 \\ E_2 \\ E_3 \end{pmatrix}, \tag{18}$$

where r_{ij} denotes the EO tensor. For a crystal with cubic symmetry such as ZnTe, only three elements of the EO tensor have non-zero value, and equal each other.

$$r_{41} = r_{52} = r_{63} \neq 0 \tag{19}$$

The index ellipsoid is described as,

$$\frac{x^2}{{n_0}^2} + \frac{y^2}{{n_0}^2} + \frac{z^2}{{n_0}^2} + 2yzr_{41}E_1 + 2zxr_{41}E_2 + 2xyr_{41}E_3 = 1 \tag{20}$$

When the electron bunch whose propagation direction is perpendicular to the (110) plane of a ZnTe crystal, the direction of the electric field impressed by the electron bunch is <001> direction. In this case, the index ellipsoid is described as equation (21).

$$\frac{x^2}{{n_0}^2}+\frac{y^2}{{n_0}^2}+2xyr_{41}E=1 \tag{21}$$

This index ellipsoid is symmetrical about the x and y axes. The eq. (21) is described as the equation (22) in the *XY* coordinate system which is rotated *xy* coordinate system by 45 degree.

$$\left(\frac{1}{{n_0}^2}-r_{41}E\right)X^2+\left(\frac{1}{{n_0}^2}+r_{41}E\right)Y^2=1\ , \tag{22}$$

If *X* and *Y* axes are the primary axes of the crystal,

$$\frac{1}{{n_X}^2}=\frac{1}{{n_0}^2}-r_{41}E, \frac{1}{{n_Y}^2}=\frac{1}{{n_0}^2}+r_{41}E\ , \tag{23}$$

When r_{41} is smaller than n_0, n_X and n_Y are described as the equation (24).

$$n_X=n_0+\frac{1}{2}{n_0}^3r_{41}E, n_Y=n_0-\frac{1}{2}{n_0}^3r_{41}E\ , \tag{24}$$

The phase shift between *X* axis and *Y* axis depends on the electric field strength.

$$\Gamma=\frac{2\pi}{\lambda}{n_0}^3r_{41}E\ , \tag{25}$$

References

[1] R. Bonifacio, and C. Pellegrini, *Opt. Commun.*, **50**, 373 (1984).

[2] K. J. Kim, *Phys. Rev. Lett.*, **57**, 1871 (1986).

[3] P. B. Corkum, Phys. Rev. Lett., 71, 1994 (1993).

[4] K. C. Kulander, K. J. Schafer, and J. L. Krause, *Proceedings of the Workshop on Super Intense Laser Atom Physics*, **316**, 95 (1993).

[5] L. DiMauro, A. Doyuran, W. Graves, R. Heese, E.D. Johnson, S. Krinsky, H. Loos, J. B. Murphy, G. Rakowsky, J. Rose, T. Shaftan, B. Sheehy, J. Skaritka, X. J. Wang, and L. H. Yu, *Nucl. Instrum. Methods Phys. Res. A*, **507** 15 (2003).

[6] G. Lambert, T. Hara, D. Garzella, T. Tanikawa, M. Labat, B. Carre, H. Kitamura, T. Shintake, M. Bougeard, S.Inoue, Y. Tanaka, P. Salieres, H. Merdji, O. Chubar, O. Gobert, K. Tahara, and M.-E. Couprie, *Nature Phys.*, **4**, 296 (2008).

[7] E. J. Takahashi, Y. Nabekawa, and K. Midorikawa, *Opt. Lett.*, **27**, 1920 (2002).

[8] E. J. Takahashi, Y. Nabekawa, M. Nurhuda, and K. Midorikawa, *J. Opt. Soc. Am. B.*, **20**, 158 (2003).

[9] E. J. Takahashi, H. Hasegawa, Y. Nabekawa, and K. Midorikawa, *Opt. Lett.*, **5**, 507 (2004).

[10] T. Togashi, E. J. Takahashi, K. Midorikawa, M. Aoyama, K. Yamakawa, T. Sato, A. Iwasaki, S. Owada, T. Okino, K. Yamanouchi, F. Kannari, A.Yagishita, H. Nakano, M. E. Couprie, K. Fukami, T. Hatsui, T. Hara, T. Kameshima, H. Kitamura, N. Kumagai, S. Matsubara, M. Nagasono, H. Ohashi, T. Ohshima, Y. Otake, T. Shintake, K. Tamasaku, H. Tanaka, T. Tanaka, K. Togawa, H. Tomizawa, T. Watanabe, M. Yabashi, and T. Ishikawa, *Opt. Express*, **19**, 317 (2011).

[11] V. L. Ginzburg, *Physica Scipta*., **T2/1**, 182 (1982).

[12] “EO-sampling based temporal overlap control system for an HH seeded FEL” S. Matsubara, A. Iwasaki, S. Owada, T. Sato, K. Ogawa, T. Togashi, E. J. Takahashi, M. Aoyama, Y. Okayasu, T. Watanabe, and H. Tomizawa, *Proceedings of International Beam Instrumentation Conference*, (Tsukuba, September, 2012).

[13] Z. Jiang, and X. -C. Zhang, *Appl. Phys. Lett.*, **72**, 1945 (1998).

[14] F. G. Sun, Z. Jiang, and X. -C. Zhang, *Appl. Phys. Lett.*, **73**, 2233 (1998).

[15] Z. Jiang, and X. -C. Zhang, *J. Quantum. Electron.*, **36**, 1214 (2000).

[16] X. Yan, A. M. MacLeod, and W. A. Gillespie, G. M. H. Knippels, D. Oepts, A. F. G. van der Meer, and W. Seidel, *Phys. Rev. Lett.*, **85**, 3404 (2000).

[17] A. L. Cavalieri, D. M. Fritz, S. H. Lee, P. H. Bucksbaum, D. A. Reis, J. Rudati, D. M. Mills, P. H. Fuoss, G. B. Stephenson, C. C. Kao, D. P. Lowney, A. G. MacPhee, D. Weinstein, R. W. Falcone, R. Pahl, J. Als-Nielsen, C. Blome, S. Dusterer, R. Ischebeck, H. Schlarb, H. Schulte-Schrepping, Th. Tschentscher, J. Schneider, O. Hignettle, F. Sette, K. Sokolowski,-Tinten, H. N. Chapman, R. W. Lee, T. N. Hansen, O. Synnergren, J. Larsson, S. Techert, J. Sheppard, J. S. Wark, M. Bergh, C. Caleman, G. Huldt, D. van der Spoel, N. Timneau, J. Hajdu, R. A. Akre, E. Bong, P. Emma, P. Krejcik, J. Arthur, S. Brennan, K. J. Gaffney, A. M. Lindenberg, K. Luening, and J. B. Hastings, *Phys. Rev. Lett.*, **94**, 114801 (2005).

[18] A.Azima, S. Duesterr, H. Schlarb, J. Feldhaus, A. Cavalieri, D. Fritz, K. Sengstock, *Proceedings of EPAC 2006, Edinburgh, Scotland*, MOPCH011 (2006).

[19] G. Berden, G. Knipples, D. Oepts, A. F. G. van der Meer, S. P. Jamison, X. Yan, A. M. MacLeod, W. A. Gillespie, J. L. Shen, *Proceedings of the 2003 Particle Accelerator Conference*, P519.

[20] I. Wilke, A. M. MacLeod, W.A. Gillespie, G. Berdern, G. M. H. Knippels, and A. F.G. van der Meer, *Phys. Rev. Lett.*, **88**, 124801 (2002).

[21] J.R. Fletcher, *Opt. Express*, **10**, 1425 (2002).

[22] G. Berden, S. P. Jamison, A. M. MacLoad, W. A. Gillespie, B. Redlich, and A. F. G. van der Merr, *Phys. Rev. Lett.*, **93**, 114802 (2004).

[23] T. Shintake, H. Tanaka, T. Hara, T. Tanaka, K. Togawa, M. Yabashi, Y. Otake, Y. Asano, T. Bizen, T. Fukui, S. Goto, A. Higashiya, T. Hirono, N. Hosoda, T. Inagaki[1], S. Inoue, M. Ishii, Y. Kim, H. Kimura, M. Kitamura, T. Kobayashi, H. Maesaka, T. Masuda, S. Matsui, T. Matsushita, X. Maréchal, M. Nagasono, H. Ohashi, T. Ohata, T. Ohshima, K. Onoe, K. Shirasawa, T. Takagi, S. Takahashi, M. Takeuchi, K. Tamasaku, R. Tanaka, Y. Tanaka, T. Tanikawa, T. Togashi, S. Wu, A. Yamashita, K. Yanagida, C. Zhang, H. Kitamura, and T. Ishikawa, *Nature Photon.*, **2**, 555 (2008).

[24] T. Shintake, H. Tanaka, T. Hara, T. Tanaka, K. Togawa, M. Yabashi, Y. Otake, Y. Asano, T. Bizen, T. Fukui, S. Goto, A. Higashiya, T. Hirono, N. Hosoda, T. Inagaki, S. Inoue, M. Ishii, Y. Kim, H. Kimura, M. Kitamura, T. Kobayashi, Noritaka Kumagai, Hirokazu Maesaka, Takemasa Masuda, S. Matsui, T. Matsushita, X. Maréchal, M. Nagasono, H. Ohashi, T. Ohata, T. Ohshima, K. Onoe, T. Sakurai, K. Shirasawa, T. Takagi, S. Takahashi, M. Takeuchi, K. Tamasaku, R. Tanaka, Y. Tanaka, T. Tanikawa, T. Togashi, S. Wu, A. Yamashita, K. Yanagida, C. Zhang, H. Kitamura, and T. Ishikawa, *Phys. Rev. ST. Accel. Beams*, **12**, 070701 (2009).

[25] K. Togawa, T. Shintake, T. Inagaki, K. Onoe, T. Tanaka, H. Baba, and H. Matsumoto, *Phys. Rev. ST. Accl. Beams*, **10**, 020703 (2007).

[26] M. Ferray, A. L'Huillier, X. F. Li, L. A. Lompre, G. Mainfray, and C. Manus, *J. Phys. B: At. Mol. Opt. Phys.*, **21** L31 (1988).

[27] G. Lambert, T. Hara, M. Labat, T. Tanikawa, Y. Tanaka, M. Yabashi, D. Garzella, B. Carre, and M. E. Couprie, *Europhys. Lett.*, **88**, 54002 (2009).

[28] A. H. Lumpkin, B. X. Yang, W. J. Berg. J. W. Lewellen, N. S. Sereno, and U.

Happek, *Nucel. Instrum. Methods Phys. Res. A*, **445**, 356 (2000).

[29] M. Richter, A. Gottwald, U. Kroth, A. A. Sorokin, S. V. Bobashev, L. A. Shmaenok, J. Feldhaus, Ch. Gerth, B. Steeg, K. Tiedtke, and R. Treusch, *Appl. Phys. Lett*., **83**, 2970 (2003).

[30] K. Tiedtkle, J. Feledhaus, U. Hahn, U. Jastrow, T. Nuneuz, T. Tschentcher, S. V. Bobashev, A. A. Sorokin, J. B. Hastings, S. Moller, L. Cibik, A. Gottwald, A. Hoehl, U. Kroth, H. Schoppe, and G. Ulm, M. Richter, *J. Appl. Phys*., **103**, 094511 (2008).

[31] N. Saito, P. N Juranic, M. Kato, M. Richter, A. A Sorokin, K. Tiedteke, U. Jastrow, H. Schoppe, M. Nagasono, M. Yabashi, K. Tono, T. Togashi, H. Kimura, H. Ohashi, and T. Ishikawa, *Metrologia*, **47**, 21 (2010).

[32] A. Yariv, and P. Yeh, *Optical waves in crystals: propagation and laser radiation*, New York, Wiley, 1984.

Chapter 3

Multiphoton ionization of atoms by free-electron laser seeded with high order harmonics of Ti:Sapphire laser

1. Introduction

Intense light sources in the EUV regions had not been available until very recently when the self-amplified spontaneous emission (SASE) type free-electron laser (FEL) was introduced [1, 2]. The SASE-FEL is a promising light source for the non-linear spectroscopy of atoms and molecules because of its wavelength tunability and high peak intensity. Indeed, the laser intensity of SASE-FEL pulses could become larger than that of the high-order harmonics of ultrashort laser pulses by more than two orders of magnitude.

Studies on the multiphoton ionization of atoms and molecules in the EUV wavelength region have been reported by using SASE-FELs. Multiple ionizations of Xe and Ar irradiated with FEL pulses of λ = 98 nm and around 10^{13} W/cm^2 were reported by Wabnitz *et al.* [3]. The input pulse intensity dependence of the ion yield of Xe^{m+} (m = 3, 4, and 5) and Ar^{n+} (n = 2, 3) were examined, and from the slope of the ion yields plotted with respect to the intensity of the input pulse on the logarithmic scale, the formation of Xe^{m+} (m = 3, 4, and 5) and Ar^{n+} (n = 2, 3) was confirmed as the sequential multiphoton ionization. The investigation of the multiphoton ionization of Xe was reported for FEL pulses at λ = 13 nm and with the intensity of 10^{12} to 10^{16} W/cm^2, and the formation of the multiply charged ions up to Xe^{21+} were reported by Solokin *et al.* [4]. The formation process of multiply charged ions was theoretically studied by solving the differential rate equations of ion yields [5, 6]. The formation of Ar^{6+} and Ar^{7+} were reported by Motomura *et al.* [7] and Sato *et al.* [8], respectively. The multiple ionization of Ne irradiated with the SASE-FEL pulses at λ = 29.1 nm and with the intensity of 10^{14} W/cm^2 was examined [9]. The multiphoton ionization of Ne with the one photon energy of 41 to 42 eV was investigated [11]. To clarify the resonance ion-

ization of Ne, the spectra of SASE-FEL pulses were measured, and the correlation between the time of flight spectra and the spectra was investigated. From the correlation between the Ne^{2+} to Ne^{+} ratio and the spectra of the SASE-FEL pulses, the increment of Ne^{2+} yields was attributed to the resonant excitation of the $2p$ - nl transition of Ne^{+}. The sequential two photon double ionization of N_2 for the SASE-FEL pulses of λ = 32 nm and 2×10^{13} W/cm^2 was reported [12]. The ionization of N_2 for the FEL pulses of λ = 50.8 nm and 10^{14} W/cm^2 were examined, and the two photon double ionization was confirmed from the observation of the Coulomb explosion of N_2^{2+} [13]. Those results suggest that the SASE-FEL pulses are intense enough to induce nonlinear optical phenomena such as multiphoton ionization.

It is true that the development of the SASE-FELs enabled us to investigate the nonlinear optical phenomena, such as the multiphoton ionization of atoms and molecules in EUV and Soft X-ray wavelength regions. However, the temporal and spectral structure of the SASE-FEL pulses exhibit spike-like structures with pulse-to-pulse fluctuations which originate from the nature of the amplification scheme of the SASE-FEL pulses. Because these spectral and temporal fluctuations cannot be reduced by any adjustments of experimental parameters such as the temporal pulse width, the central wavelength and the laser intensity, interpretations of the multiphoton ionization processes of atoms and molecules induced by these SASE-FEL pulses in EUV and Soft X-ray wavelength regions are difficult. The improvement of the temporal and spectral coherence of the SASE-FEL pulses would be important to investigate the ionization processes of atoms and molecules.

In the present study, the 13th order harmonic pulses of Ti:Sapphire laser were amplified up to 20 μJ/pulse for as long as 7 hours by introducing a real-time and

non-destructive timing monitor to monitor the timing drift between two pulses by using an electro-optic (EO) sampling technique. The two photon ionization of He was investigated.

2. Experiments

The fundamental output pulses of a Ti:sapphire laser (800 nm, 30 mJ/pulse, 150 fs FWHM, 30 Hz) were loosely focused using a plano-convex lens (f = 4 m) into a Xe gas cell placed in a vacuum chamber to generate the 13th order harmonic at 61.5 nm. The generated harmonic pulses were spatially separated from the fundamental laser pulses (800 nm) by a pair of SiC mirrors and focused by two Pt concave mirrors into the undulator part of the SCSS test accelerator, where the injected high-order harmonic pulses were overlapped temporally and specially with electron bunches (0.4 nC/bunch) accelerated at 250 MeV. In order to amplify the input high-order harmonic pulses through the seeding process, the undulator gap was adjusted and optimized for the 13th order harmonic.

For the synchronization of the high-order harmonic pulses and the electron bunches, the timing drift was monitored by the EO sampling technique and was adjusted by varying the triggering timing for the seeding laser through a home-built feedback system. As a result, the timing drift was successfully reduced to within 1 ps, and consequently, the stable generation of high-order harmonic seeded FEL pulses was achieved for a period as long as 7 hours, and the seeding probability, defined by the ratio of the number of the seeded pulses with respect to the number of the non-seeded SASE FEL pulses, was raised significantly to as much as 20%.

Figure 1 shows the schematic drawing of the experimental setup for the inves-

tigation of the multiphoton ionization process. The seeded FEL pulses were reflected by two steering mirrors coated with SiC, and introduced into the home-built TOF mass spectrometer. The seeded FEL pulses were focused onto a sample gas jet by two cylindrical mirrors (f = 1000 mm) coated with SiC [14]. The gas jet was introduced into the vacuum chamber from a pulsed valve through a skimmer with the orifice diameter of 0.5mm. The generated ions were mass separated by the Wily-Maclaren type TOF mass spectrometer [15], detected by microchannel plates, and recorded by an oscilloscope (DPO7254C, Tektronix). The seeded FEL pulses and the SASE-FEL pulses were horizontally polarized, which made them parallel to the TOF axis.

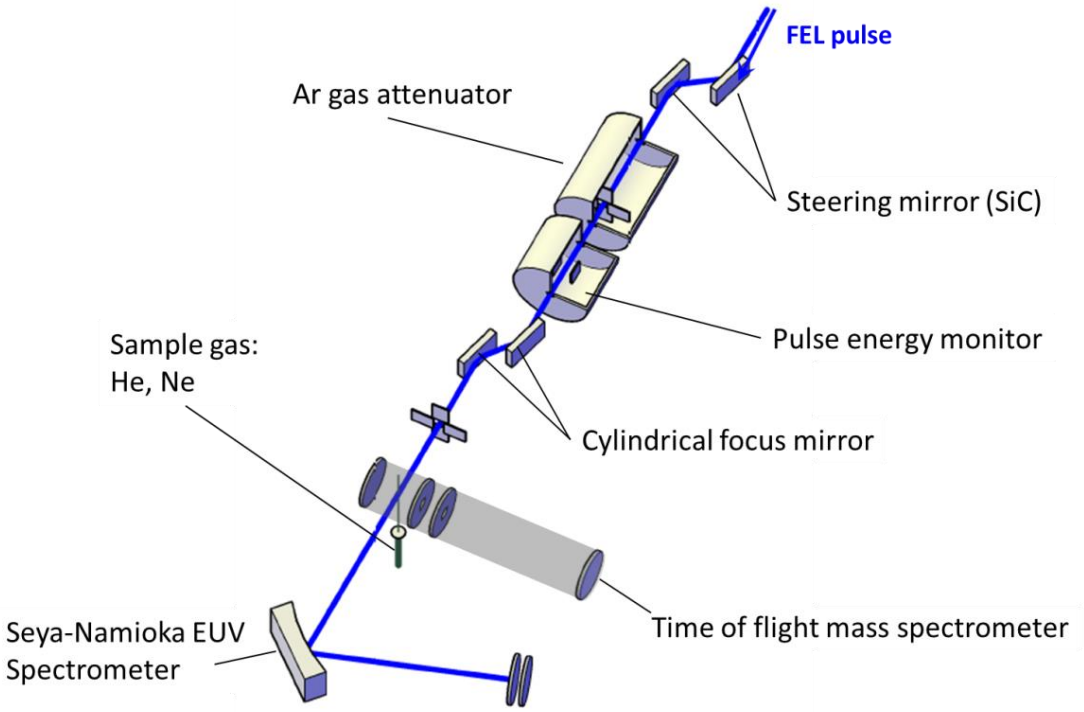

Figure 1. The experimental setup for the observation of the multiphoton ionization of atoms.

3. Results and Discussion

3.1. Ion yield of He^+

Figure 2 shows the time of flight mass spectra of He which was obtained by averaging over 3000 shots. He^+ was observed at *m/z* = 4, and He^{2+} was observed at *m/z* = 2. H_2^+ originating from the residual H_2O in the vacuum chamber was also observed at *m/z* = 2. He^{2+} and H_2^+ could not be distinguished from the TOF mass spectra alone.

3.2. Intensity dependence of He^+ yield

In Fig. 3, the yields of the He^+ ions recorded when the He gas was irradiated with the seeded FEL pulses and the non-seeded SASE FEL pulses are respectively plotted as a function of their pulse energy. Because the first ionization potential of He is 24.6 eV and the photon energies of the high-order harmonic seeded FEL and non-seeded SA-SE-FEL pulses are 20.2 eV [16], two photons are required to ionize He.

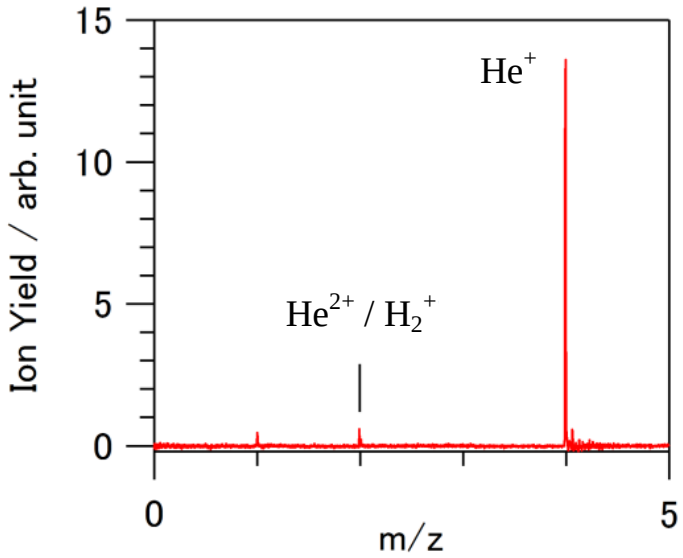

Figure 2. The averaged mass spectrum of He^+ for 3000 shots. He^+ was observed at m/z = 4. He^{2+} and H_2^+ were observed at *m/z* = 2. H_2^+ was emitted from the residual H_2O.

The energy diagram of He is shown in Fig. 4, confirming the non-resonant two photon ionization. As shown in Fig. 3, the slopes of the He^+ yield were determined as n = 2.0(1) and 1.9(1) when the seeded and non-seeded FEL pulses were adopted, respectively, showing that He atoms are ionized by a non-resonance two-photon ionization process.

Considering that He^+ ions are generated by a non-resonant two-photon absorption process, the larger He^+ ion yield obtained with the seeded pulses than that obtained with the non-seeded pulses, as shown in Fig. 3, should reflect the larger peak energy, or equivalently, the narrower pulse width of the seeded pulses than the non-seeded pulses.

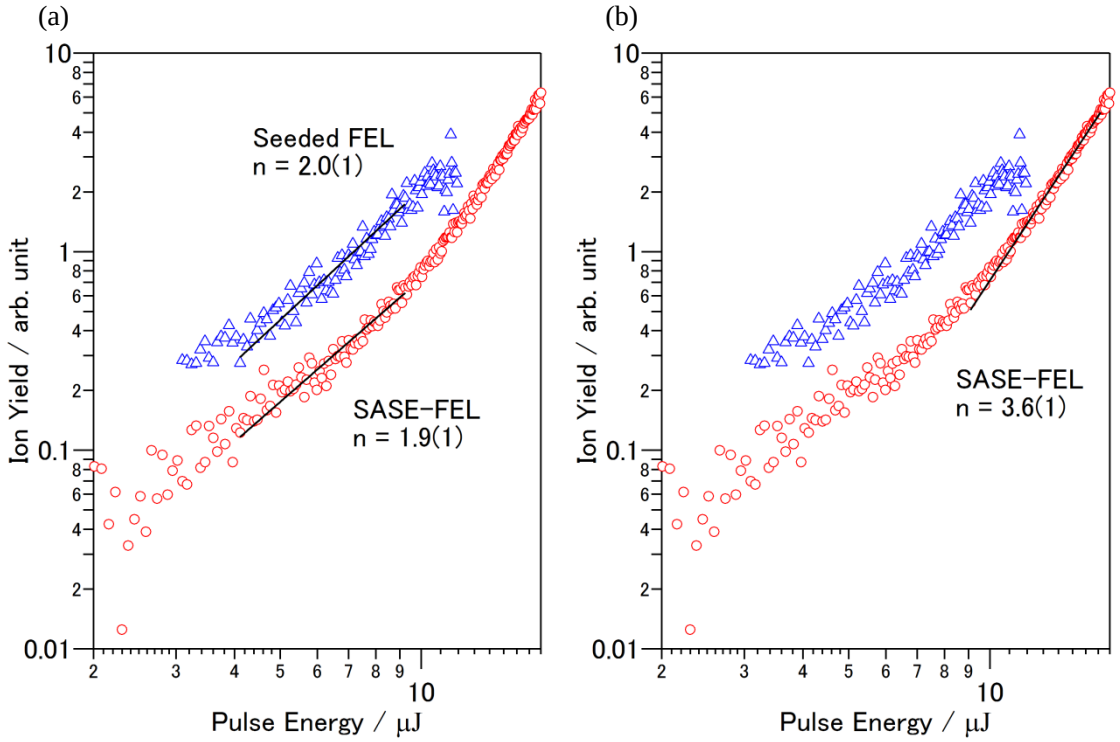

Figure 3. (a) Input pulse energy dependence of He^+ yield for seeded FEL (blue triangles), and SASE-FEL (red circles). (b) The energy dependence of the He^+ yields showed slope of n = 3.6(1) at 5 to 8 μJ energy region.

From the spectrum of the seeded FEL pulse, its pulse duration is estimated to be 46(1) fs, assuming that the Fourier transformed limited pulses were generated, which is consistent with the pulse duration (50 fs) of the input high-order harmonic pulses. The following equation represents the He^+ yields:

$$Y_{\mathrm{He}^+} = \eta \cdot N_{\mathrm{He}} \cdot \sigma_{\mathrm{He}}^{(2)} \cdot \left(\frac{\lambda I}{hc}\right)^2 \cdot \tau = N_{\mathrm{He}} \cdot \sigma_{\mathrm{He}}^{2} \cdot \left(\frac{\lambda E}{hcS}\right)^2 \cdot \frac{1}{\tau}\ , \tag{1}$$

where η denotes the detection efficiency of our experimental apparatus, N_{He} denotes the number of He atoms in the interaction region, I denotes the focused intensity of the FEL pulse, E denotes the pulse energy, S denotes the cross section of the FEL pulse at the focal point, and τ denotes the temporal width of the FEL pulse. Then, the ratio of the ion yields for the seeded FEL pulse to the ion yields for the SASE-FEL is described as

$$\frac{Y_{\mathrm{He}^+(Seed\ FEL)}}{Y_{\mathrm{He}^+(SASE\ FEL)}} = \frac{\tau_{SASE\ FEL}}{\tau_{Seed\ FEL}}\ . \tag{2}$$

From the pulse duration of the seeded output (46 fs) and the ratio of the He^+ ion yield (~ 2.7), the pulse duration of the non-seeded SASE FEL output is estimated to be 125 fs, which is in agreement with an estimate of the pulse duration of the SA-SE-FEL output, which was in the range between 100 fs and 150 fs.

The slope of the SASE-FEL pulse was found to be 3.5 above 10 μJ/pulse, showing that a higher non-linear ionization proceeded through above threshold ionization (ATI) and/or absorption to the two electron excited states located around 63.12 eV [16] by the three photon energy region. The resonant three photon ionization achieved by using photoelectron spectroscopy at 51.4 nm SASE-FEL pulses was reported by Hishikawa *et al.*, suggesting an above threshold ionization via two-electron excited states [17]. The increase of the slope is not significant for the amplified FEL pulses,

due to the narrow bandwidth, estimated to be 0.06 nm (FWHM), limited by the seeding harmonic laser pulses.

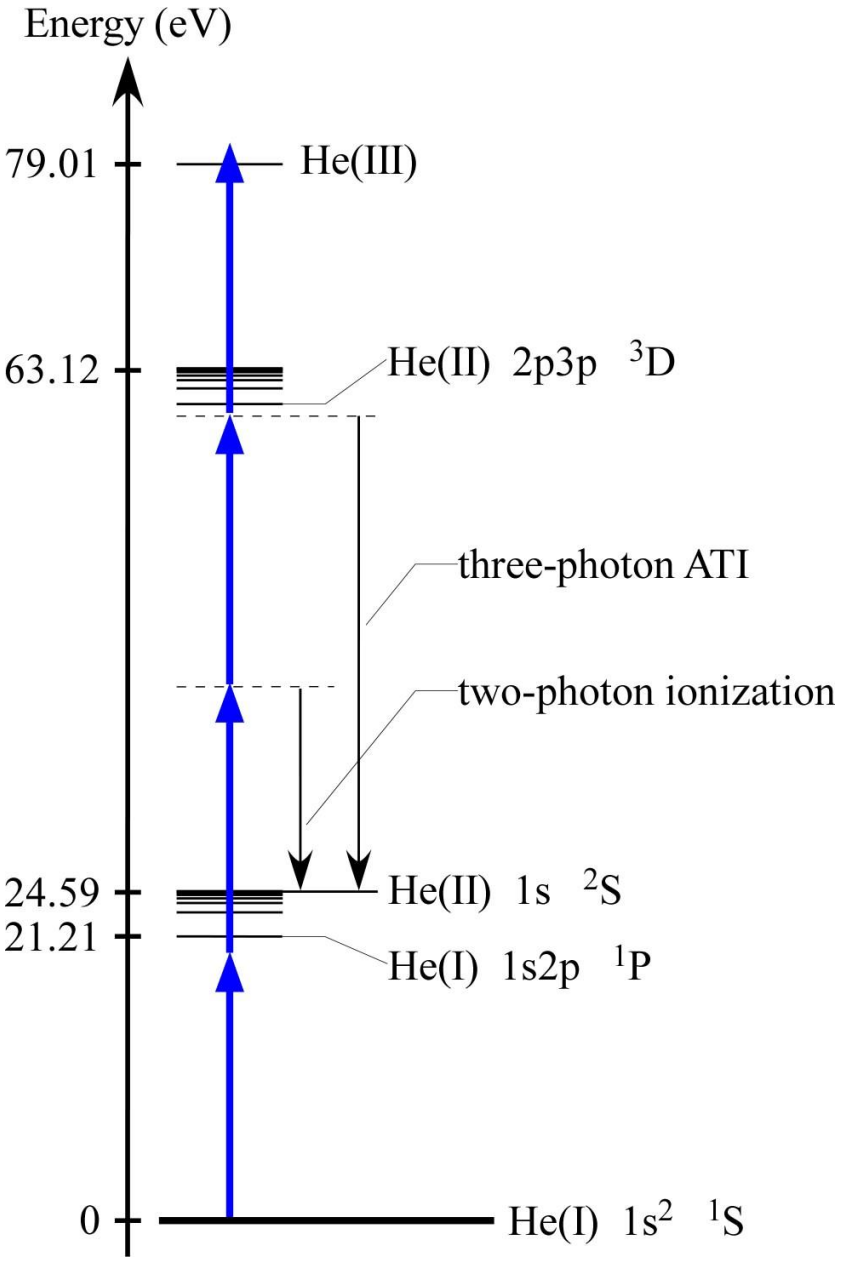

Figure 4. Energy diagram of He^+ and He^{2+}.

4. Conclusion

The multiphoton ionization of He was examined for the FEL pulses seeded with the 13th order harmonics of Ti:Sapphire laser pulses. The multiphoton ionization for the SASE-FEL pulses with the same pulse energy was also examined for comparison. The formation of He^+ was confirmed to be non-resonant two photon ionization, and the difference between the temporal width of the seeded FEL pulse and the SASE-FEL pulse contributed to the He^+ yields. This means that the laser intensity of the seeded FEL pulses is 2.7 times higher than the laser intensity of the SASE-FEL pulses.

References

[1] W. Ackermann, G. Asova, V. Ayvazyan, A. Azima, N. Baboi, J. Bahr, V. Balandin, B. Beutner, A. Brandt, A. Bolzmann, R. Brinkmann, O. I. Brovko, M. Castellano, P. Castro, L. Catani, E. Chiadroni, S. Choroba, A. Cianchi, J. T. Costello, D. Cubaynes, J. Dardis, W. Decking, H. Delsim-Hashemi, A. Delserieys, G. Di Pirro, M. Dohlus, S. Düsterer, A. Eckhardt, H. T. Edwards, B. Faatz, J. Feldhaus, K. Flöttmann, J. Frisch, L. Fröhlich, T. Garvey, U. Gensch, Ch. Gerth, M. Görler, N. Golubeva, H.-J. Grabosch, M. Grecki, O. Grimm, K. Hacker, U. Hahn, J. H. Han, K. Honkavaara, T. Hott, M. Hüning, Y. Ivanisenko, E. Jaeschke, W. Jalmuzna, T. Jezynski, R. Kammering, V. Katalev, K. Kavanagh, E. T. Kennedy, S. Khodyachykh, K. Klose, V. Kocharyan, M. Körfer, M. Kollewe, W. Koprek, S. Korepanov, D. Kostin, M. Krassilnikov, G. Kube, M. Kuhlmann, C. L. S. Lewis, L. Lilje, T. Limberg, D. Lipka, F. Löhl, H. Luna, M. Luong, M. Martins, M. Meyer, P. Michelato, V. Miltchev, W. D. Möller, L. Monaco, W. F. O. Müller, O. Napieralski, O. Napoly, P. Nicolosi, D. Nölle, T. Nuñez, A. Oppelt, C. Pagani, R. Paparella, N. Pchalek, J. P. Gutierrez, B. Petersen, B. Petrosyan, G. Petrosyan, L. Petrosyan, J. Pflüger, E. Plönjes, L. Poletto, K. Pozniak, E. Prat, D. Proch, P. Pucyk, P. Radcliffe, H. Redlin, K. Rehlich, M. Richter, M. Roehrs, J. Roensch, R. Romaniuk, M. Ross, J. Rossbach, V. Rybnikov, M. Sachwitz, E. L. Saldin, W. Sandner, H. Schlarb, B. Schmidt, M. Schmitz, P. Schmüser, J. R. Schneider, E. A. Schneidmiller, S. Schnepp, S. Schreiber, M. Seidel, D. Sertore, A. V. Shabunov, C. Simon, S. Simrock, E. Sombrowski, A. A. Sorokin, P. Spanknebel, R. Spesyvtsev, L. Staykov, B. Steffen, F. Stephan, F. Stulle, H. Thom, K. Tiedtke, M. Tischer, S. Toleikis, R. Treusch, D. Trines, I. Tsakov, E. Vogel, T. Weiland, H. Weise, M. Wellhöfer, M. Wendt, I. Will, A. Winter, K. Wittenburg, W.

Wurth, P. Yeates, M. V. Yurkov, I. Zagorodnov, and K. Zapfe *Nat. Phys.*, **1**, 336 (2007).

[2] T. Shintake, H. Tanaka, T. Hara, T. Tanaka, K. Togawa, M. Yabashi, Y. Otake, Y. Asano, T. Bizen, T. Fukui, S. Goto, A. Higashiya, T. Hirono, N. Hosoda, T. Inagaki[1], S. Inoue, M. Ishii, Y. Kim, H. Kimura, M. Kitamura, T. Kobayashi, H. Maesaka, T. Masuda, S. Matsui, T. Matsushita, X. Maréchal, M. Nagasono, H. Ohashi, T. Ohata, T. Ohshima, K. Onoe, K. Shirasawa, T. Takagi, S. Takahashi, M. Takeuchi, K. Tamasaku, R. Tanaka, Y. Tanaka, T. Tanikawa, T. Togashi, S. Wu, A. Yamashita, K. Yanagida, C. Zhang, H. Kitamura, and T. Ishikawa, *Nat. Photon*., **2**, 555 (2008).

[3] H. Wabnits, A. R. B. de Castro, P. Gurtler, T. Laarmann, W. Laasch, J. Schulz, and T. Moller, *Phys. Rev. Lett.*, **94**, 023001 (2005).

[4] A. A. Sorokin, S. V. Bobashev, T. Feigl, K. Tiedtke, H. Wabnitz, and M. Richter, *Phys. Rev. Lett.*, **99**, 213002 (2007).

[5] M. G. Makris, P. Lambropouls, and A. Mihelic, *Phys. Rev. Lett.*, **102**, 033002 (2009).

[6] P. Lambropouls, K. G. Papamihail, and P. Decleva, *J. Phys. B: At. Mol. Opt. Phys.*, **44**, 175402 (2011).

[7] K. Motomura, H. Fukuzawa, L. Foucar, X. -J. Liu, G. Prumper, K. Ueda, N. Saito, H. Iwayama, K. Nagaya, H. Murakami, M. Yao, A. Belkacem, M. Nagasono, A. Higashiya, M. Yabashi, T. Ishikawa, H. Ohashi, and H. Kimura, *J. Phys. B*, **42**, 221003 (2009).

[8] T. Sato, A. Iwasaki, T. Okino, K. Yamanouchi, A. Yagishita, H. Yazawa, F. Kannari, M. Aoyama, K. Yamakawa, K. Midorikawa, H. Nakano, M. Yabashi, M. Nagasono, A. Higashiya, T. Togashi, and T. Ishikawa, *Rev. Laser Eng.*, **37**, 905 (2009).

[9] A. A. Sorokin, M. Wellhofer, S. V. Bobashev, K. Tiedtke, and M. Richter, *Phys. Rev. A*, **75**, 051402 (2007).

[10] M. Martins, M. Wellhofer, A. A. Sorokin, M. Richter, K. Tiedtke, and W. Wurth, *Phys, Rev. A*, **80**, 023411 (2009).

[11] M. Richter, S. V. Bobashev, A. A. Sorokin, and K. Tidetke, *J. Phys. B: Mol. Opt. Phys.*, **43**, 194005 (2010).

[12] A. A. Sorokin, S. V. Babashev, K. Tiedtke, and M. Richer, *J. Phys. B: Mol. Opt. Phys.*, **39**, L299 (2006).

[13] T. Sato, T. Okino, K. Yamanouchi, A. Yagishita, F. Kannari, K. Yamakawa, K. Midorikawa, H. Nakano, M. Yabashi, M. Nagasono, and T. Ishikawa, *Appl. Phys. Lett.*, **92**, 154103 (2008).

[14] H. Ohashi, Y. Senba, M. Nagasono, M. Yabashi, K. Tono, T. Togashi, T. Kudo, H. Kishimoto, T. Miura, H. Kimura, and T. Ishikawa, *Nucl. Instrum. Meth. A*, **649**, 163 (2011).

[15] W. C. Wiley, and I. H. Mclaren, *Rev. Sci. Instrum.*, **26**, 1150 (1955).

[16] W. C. Martin, *J. Phys. Chem. Ref. Data*, **2**, 257 (1973).

[17] A. Hishikawa, M. Fushitani, Y. Hikosaka, A. Matsuda, C. -N. Liu, T. Morishita, E. Shigemasa, M. Nagasono, K. Tono, T. Togashi, H. Ohashi, H. Kimura, Y. Senba, M. Yabashi, and T. Ishikawa, *Phys. Rev. Lett.*, **107**, 243003 (2011).

Chapter 4

Amplified spontaneous $C^3\Pi_u$ - $B^3\Pi_g$ emission and rotational and vibrational state distributions in $C^3\Pi_u$ state of N_2 in femtosecond laser induced filament in air

1. Introduction

The femtosecond laser induced filament in air is known to be formed by the balance between the self-focusing and defocusing of light by the plasma produced by ionization of atoms and molecules in air [1 - 5]. Because of this balance the intensity inside the filament becomes high while the beam propagation and the light field intensity of laser induced filament is known to be kept around 5×10^{13} W/cm^2 [1, 6, 7] in air, and this phenomenon is so called intensity clamping. As the intense femtosecond laser pulses propagate in the filament in air, the broadening of the spectrum of the pulse occurs as a result of self-phase modulation. The pulse duration of the broadband white light was reported, and the optical pulse width was found as short as few optical cycles by combining conventional pulse compression technique [8, 9]. The improvement of the spatial mode of the beam after the femtosecond filament was also reported [10], and the cleaning of the spatial mode in the filament was called self-spatial filtering [11]. The intense femtosecond laser was launched to the sky and white light was generated from filament. The white light was applied to the remote sensing in atmosphere based on the light detection and ranging (LIDAR) techniques [12]. The few-cycle pulses generated by the four-wave mixing process in the filament was reported, and low fluctuation of the intensity of the few-cycle pulses in visible wavelength region was found due to the intensity clamping [13]. Furthermore, the filament has been regarded as an attractive phenomenon by a variety of its applications such as triggering of electric discharge [14], third harmonic generation [15], and THz generation [16].

By recording emission spectra of laser induced filaments in air, Chin and his co-workers [17, 18] showed that the fluorescence emits from electronically excited N_2 as well as from electronically excited molecular ions such as N_2^+. Based on the meas-

urements of the fluorescence of the $C^3\Pi_u$ - $B^3\Pi_g$ (0, 1) transition of N_2 at 357 nm, they found that the intensity of the fluorescence propagating in the direction opposite to the laser propagation direction increased exponentially as a function of the gain medium length that they estimated from the input pulse energy, and obtained the optical gain of the fluorescence emitted towards the backward direction by regarding the filament as a uniformly excited gain medium [19].

In the present study, in order to explain the exponential increase in the intensity of the fluorescence emitted from the filament, we adopted a one-dimensional model for the amplified spontaneous emission (ASE) by assuming that the Gaussian spatial density distribution of N_2 in the $C^3\Pi_u$ state along the laser propagation direction. Furthermore, in order to investigate excitation processes of molecules in the filament, the population distributions in the vibrational and rotational levels of N_2 in the C state were investigated by the spectroscopic analyses of the fluorescence emitted from the filament in the direction perpendicular to the laser propagation axis, and were found to be expressed well by the vibrational and rotational temperatures.

2. Experiment

The output of a Ti:Sapphire laser system with the pulse duration of 47 fs (full-width at half-maximum) and a maximum energy of 20 mJ/pulse at λ = 810 nm was reflected by a multilayer-coated fused silica plate with high reflectivity at 800 nm, and focused into air to generate the filament with a lens (f = 1000 mm). A half wave plate and a polarizer were placed before the two-pass amplifier to vary the output pulse energy in the range between 0.5 and 6.0 mJ by adjusting the rotational angle of the half wave plate. The beam radius, defined as the distance from the beam center to the point where the inten-

sity of the beam decreased to $1/e^2$ of the intensity at the beam center, was 14 mm before the focusing lens.

A Czerny−Turner type spectrometer equipped with an intensified charge coupled device (ICCD) camera was used to measure the spatial images of the filament and the spectra of the fluorescence emitted from the filament. The image of the side view of the filament was projected at the entrance slit of the spectrometer by a pair of lenses, and was recorded by the ICCD camera as the zero-th order diffraction. The filament images of the fluorescence ranging from the visible and ultraviolet wavelength regions were recorded. The backward fluorescence emission passing through the multi-layer-coated fused silica plate was focused by a lens (f = 100 mm) at the acceptance surface of the fiber bundle connected to the entrance slit of the spectrometer. The backward fluorescence at around 337 nm originated from the $C^3\Pi_u$ - $B^3\Pi_g$ (0, 0), (1, 1), (2, 2) and (3, 3) transitions of N_2 was recorded by the ICCD camera, with the exposure time of around 20 ns. The experimental setups were shown in Figs.1 and 2.

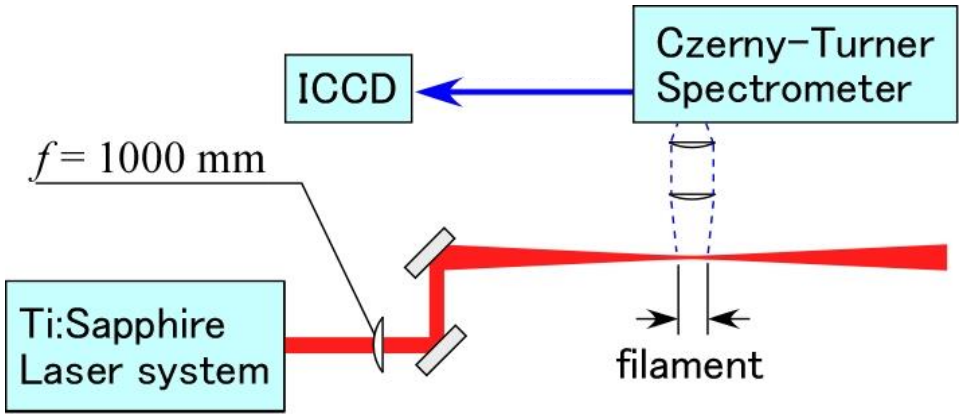

Figure 1. The experimental setup for the measurement of the side fluorescence and the image of the filament.

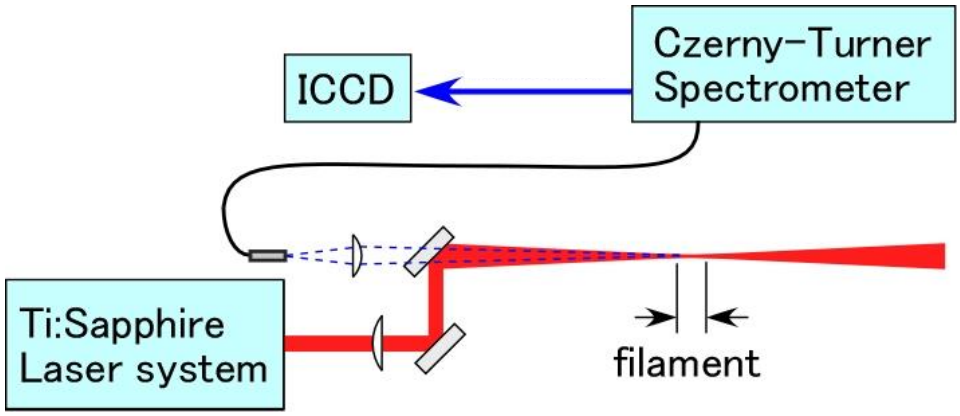

Figure 2. The experimental setup for the measurement of the backward fluorescence.

3. Results and Discussion

3.1. Measurement of the filament length

The filament images recorded at the input pulse energies of 1.0 and 6.0 mJ/pulse are shown in the upper part of Figs. 1(a) and 1(b), respectively. The fluorescence detected here is originated mainly from the $C^3\Pi_u$ - $B^3\Pi_g$ transitions at 337 nm (0, 0) and 357 nm (0, 1) of N_2, and the $B^2\Sigma_u^+$ - $X^2\Sigma_g^+$ transitions of N_2^+ at 391 nm (0, 0) and 428 nm (0, 1) [17, 18]. After integrating the fluorescence intensity of the filament images along the vertical direction in Fig. 1, the one-dimensional Gaussian-type intensity profiles were obtained as shown in the lower part of Figs. 3(a) and 3(b). Considering that the profiles were well described by a Gaussian distribution, the length of the filament was defined in the present study as the width of the Gaussian distribution at the $1/e^2$ intensity of the maximum. By recording the filament images at the 12 different input pulse energies in the intensity range between 0.5 and 6.0 mJ/pulse at intervals of 0.5 mJ/pulse, the variation of the filament length as a function of the laser pulse energy was obtained as shown in Fig. 4. As seen in Fig. 4, the filament length tends to increase almost linearly as the laser pulse energy increases.

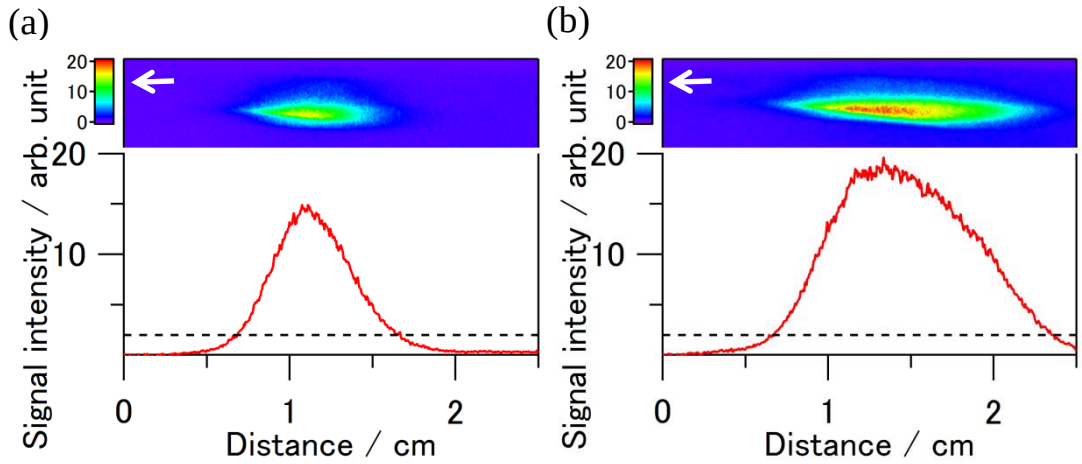

Figure 3. The ICCD images of the filament and the intensity profiles (solid line) along the filament when the pulse energies are (a) 1.0 mJ/pulse and (b) 6.0 mJ/pulse. The horizontal axis is taken along the laser propagation direction. The dashed lines are the $1/e^2$ intensity of the maximum signal intensity. The filament lengths are determined to be 8 mm and 19 mm in (a) and (b), respectively.

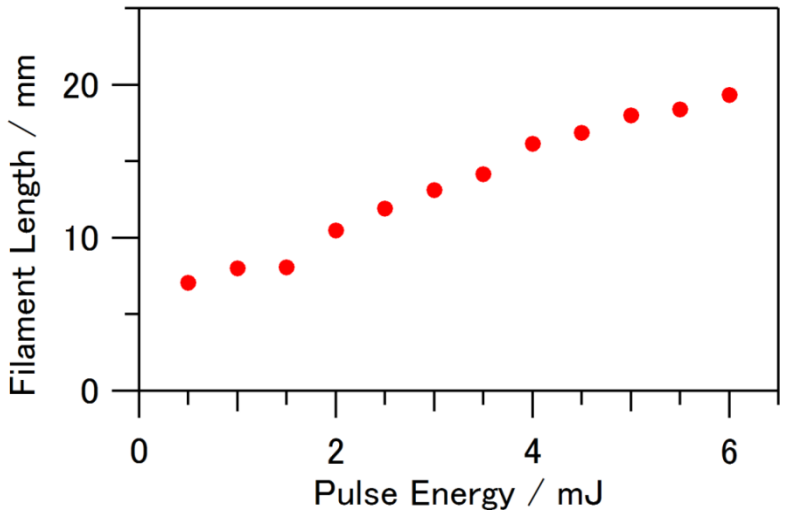

Figure 4. The experimentally determined filament lengths plotted as a function of the input pulse energy.

3.2. Backward fluorescence intensity

The intensity of the fluorescence emitted from the filament towards the backward direction, plotted in Fig. 5 as a function of the filament length, exhibits an exponential in-

crease. In order to explain this exponential increase of the backward fluorescence, a one-dimensional model of ASE described by the differential equation introduced in Ref. [20],

$$\frac{\mathrm{d}I}{\mathrm{d}z} = P(z) + g(z)I(z), \tag{1}$$

is adopted, where $P(z)$ represents the intensity of the spontaneous emission along the z axis, which is the laser propagation axis, $I(z)$ the total fluorescence intensity emitted from the filament along the z axis, and $g(z)$ the optical gain. The product of $g(z)$ and $I(z)$, that is, $g(z)I(z)$, represents the intensity of the stimulated emission. In the previous study [16], the filament was assumed to be a medium in which excited atomic and/or molecular species are uniformly distributed, and $P(z)$ and $g(z)$ were considered to be constant along the filament.

In the present study, considering the observation that the intensity distributions of the fluorescence emitted from the filament along the z direction, in the wavelength range covering the visible and ultraviolet regions, were represented well by a Gaussian-type function, both the population of N_2 in the C state and that in the B state along the filament were assumed to take a Gaussian-type distribution represented respectively by

$$N_{\mathrm{C}}(z) = N_{\mathrm{C},0} \exp(-z^2 / w^2), \tag{2}$$

$$N_{\mathrm{B}}(z) = N_{\mathrm{B},0} \exp(-z^2 / w^2), \tag{3}$$

where w denotes the width at the 1/e intensity of the maximum corresponding to the filament length divided by $2\sqrt{2}$, $N_{C,0}$ and $N_{B,0}$ denote respectively the maxima of the population distribution of N_2 in the C and B state. By using these distributions, the optical gain $g(z)$ is represented as

$$\begin{aligned} g(z) &= \sigma_{CB}\{N_C(z) - N_B(z)\} \\ &= \sigma_{CB}\{N_{C,0} - N_{B,0}\}\exp(-z^2/w^2), \end{aligned} \tag{4}$$

where σ_{CB} denotes the cross section of the stimulated emission. On the other hand, the distribution of the spontaneous emission along the z axis is represented as

$$\begin{aligned} P(z) &= h\nu A_{CB} N_C(z) \\ &= h\nu A_{CB} N_{C,0}\exp(-z^2/w^2), \end{aligned} \tag{5}$$

where A_{CB} denotes the Einstein A coefficient for the C-B transition. By substituting Eqs. (4) and (5) into Eq. (1),

$$\frac{dI}{dz} = \{h\nu A_{CB} N_{C,0} + \sigma_{CB}(N_{C,0} - N_{B,0})I(z)\}\exp(-z^2/w^2), \tag{6}$$

is obtained.

By solving the differential equation Eq. (6) numerically for a given value of $\sigma_{CB}(N_{C,0}\text{-}N_{B,0})$, the intensities of the backward fluorescence can be derived. By comparing the calculated intensities obtained with different values of $\sigma_{CB}(N_{C,0}\text{-}N_{B,0})$ with the experimental results in the input pulse energy range between 0.5 and 6.0 mJ/pulse, an

optimized value of $\sigma_{CB}(N_{C,0}\text{-}N_{B,0})$ was obtained. The best-fit results are plotted with the blue circles in Fig. 5 as a function of the observed filament length. In Eq. (6), $h\nu A_{CB}N_{C,0}$ represents the observed intensity and w is the observed width of a Gaussian fluorescence intensity distribution along z axis. As shown in Fig. 5, this simulated results reproduces well the experimental data as long as $N_{C,0}$ is larger than $N_{B,0}$. This shows that the population inversion was realized between the $C^3\Pi_u$ and the $B^3\Pi_g$ states of N_2 in the laser induced filament, and that the exponential increase in the fluorescence intensity can be ascribed to the ASE.

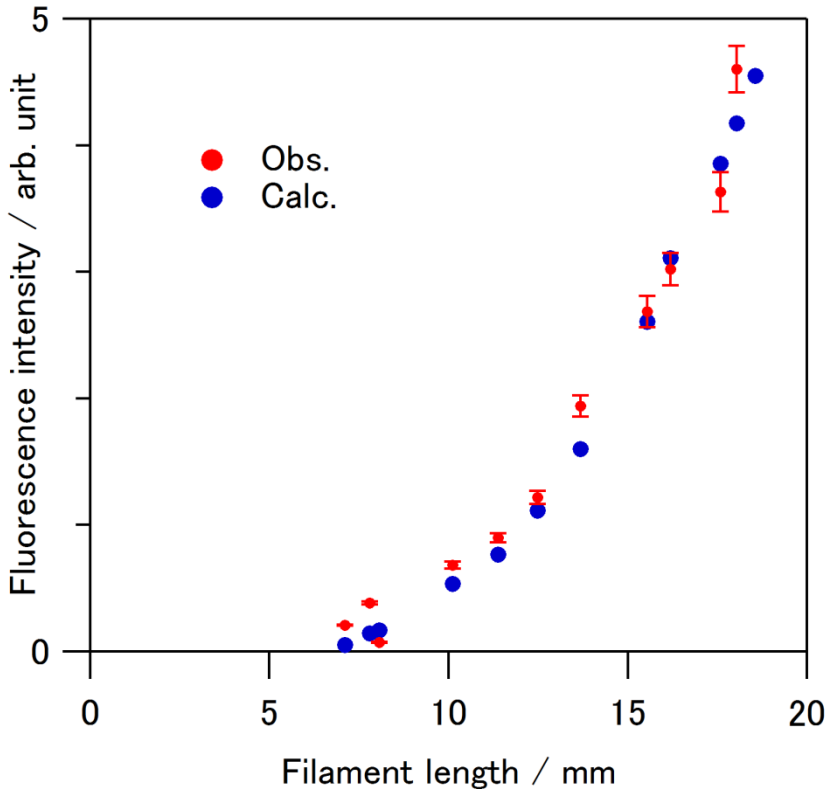

Figure 5. The observed backward fluorescence intensity (red circle), and the calculated backward fluorescence intensity (blue circle).

3.3. Vibrational temperature

The $C^3\Pi_u$ - $B^3\Pi_g$ emission spectrum of N_2 recorded from the side of the filament is shown in Fig. 6, in which the sequence of the transitions assigned to (v, v) = (0, 0), (1, 1), (2, 2), and (3, 3) can be identified. If the population in the respective vibrational levels in the C state can be represented by a Boltzmann distribution with the vibrational temperature T_v, the ratio of the intensity of the C-B (v, v) transition, $I_{v,v}$, with respect to the C-B (0, 0) transition, $I_{0,0}$, can be expressed as

$$\frac{I_{v,v}}{I_{0,0}} = \frac{\left|\langle \psi_v' | \psi_v'' \rangle\right|^2}{\left|\langle \psi_0' | \psi_0'' \rangle\right|^2} \frac{{\nu_{v,v}}^4}{{\nu_{0,0}}^4} \exp\left(-\frac{\Delta E_v}{kT_v}\right), \tag{7}$$

where $\left|\langle \psi_v' | \psi_v'' \rangle\right|^2$ and $\nu_{v,\,v}$ are the Franck-Condon factor and the transition wave-number of the C-B (v, v) transition [21], and ΔE_v represents the vibrational term value of the vibrational level in the C state whose vibrational quantum number is v.

By defining R_v as

$$R_v = -\ln\left[\left(\frac{I_{v,v}}{I_{0,0}}\right)\left(\frac{\left|\langle \psi_v' | \psi_v'' \rangle\right|}{\left|\langle \psi_0' | \psi_0'' \rangle\right|}\right)^2\left(\frac{\nu_{v,v}}{\nu_{0,0}}\right)^4\right],$$

$$= -\frac{\Delta E_v}{kT_v}, \tag{8}$$

the R_v values are calculated for v = 1, 2, and 3 using the experimental values of $I_{v,v}$ and $I_{0,0}$ obtained when the input pulse energy was 6.0 mJ/pulse, and are plotted in Fig. 7 as a function of ΔE_v. From a least-squares fit to Eq. (8), the vibrational temperature was

determined to be T_v = 2650(200) K.

By using the data taken at different input pulse energies in the range between 0.5 and 5.5 mJ/pulse, the vibrational temperatures were obtained through the same procedure as above, and the resultant vibrational temperatures were obtained as plotted in Fig. 8. As shown in Fig. 8, the experimental vibrational temperature takes almost constant values distributing in the narrow temperature range between 2600 and 3000 K, indicating that the population distribution in the respective vibrational states in the C state of N_2 in the filament tends to take almost the same values in the wide range of the input laser pulse energy, which can be ascribed to the clamping of the laser field intensity in the filament [1, 6, 7].

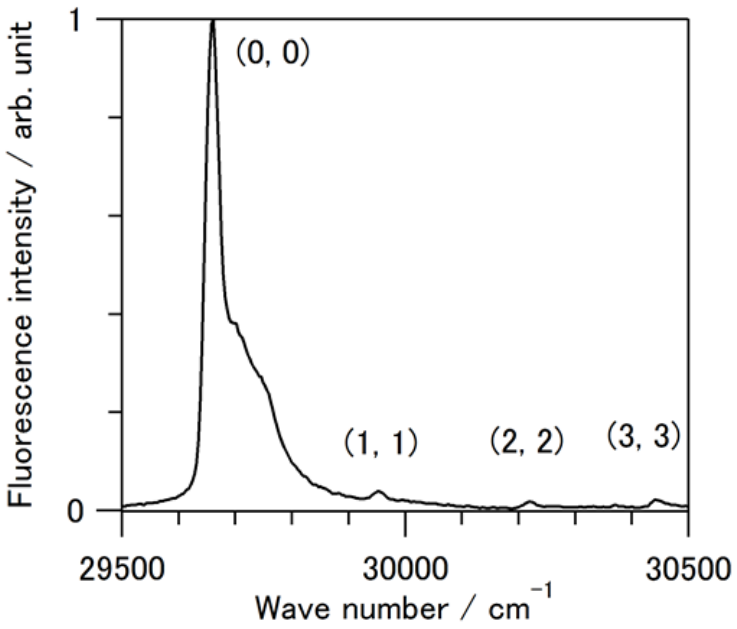

Figure 6. The emission spectrum the C-B(v, v) fluorescence of N_2 measured from the side of the filament when the input laser pulse energy was 6 mJ/pulse.

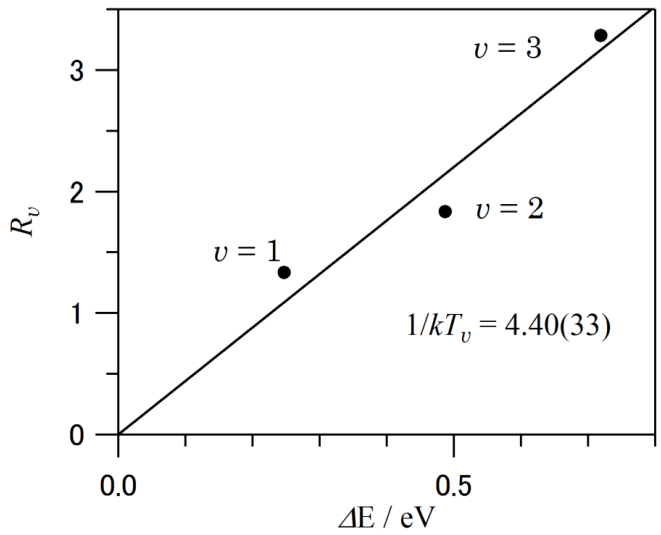

Figure 7. R_υ defined by Eq. (8) plotted as a function of the vibrational term values for υ = 1, 2 and 3 when the input pulse energy was 6.0 mJ.

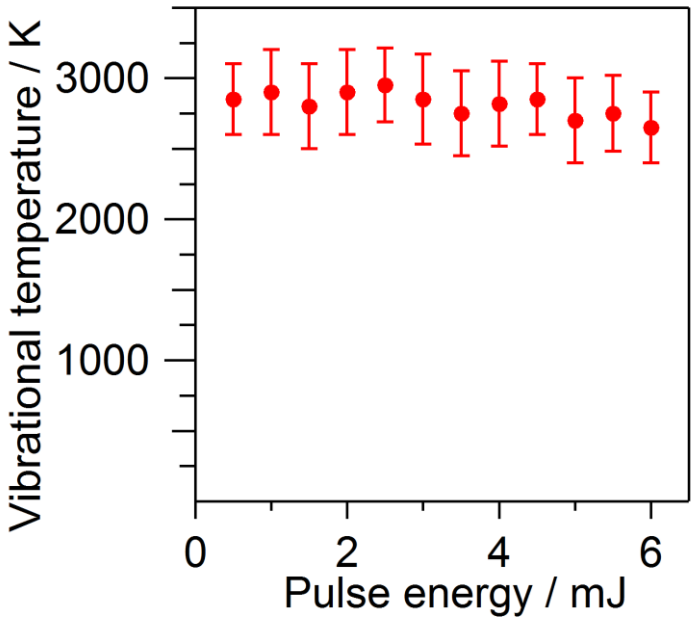

Figure 8. The dependence of the vibrational temperature of N_2 in the C state on the input laser pulse energy.

3.4. Rotational temperature

As shown in Fig. 4, the respective emission peaks are shaded towards the higher wave number side. These profiles can be ascribed to a rotational structure of the C $^3\Pi_g$ - $B^3\Pi_u$ (v, v) transitions. The rotational structure of the $C^3\Pi_g$ - $B^3\Pi_u$ transition of N_2 split into three sub-bands corresponding to the $^3\Pi_2$ - $^3\Pi_2$, $^3\Pi_1$ - $^3\Pi_1$, and $^3\Pi_0$ - $^3\Pi_0$ transitions in the P and R branches and two sub-bands corresponding to $^3\Pi_2$ - $^3\Pi_2$ and $^3\Pi_1$ - $^3\Pi_1$ in the Q branch [22]. A subscript attached to the term symbols in the sub-band transitions represents the quantum number Ω, the sum of the sum of the projection of the electronic orbital angular momentum and the projection of the spin angular momentum.

The wave numbers of respective transitions can be expressed by the Dunham expansion [22] as

$$\nu^{\mathrm{C}_{v,J'}}_{\mathrm{B}_{v,J''}} = \sum_{p=0}^{2}\sum_{q=0}^{2}\{Y^{\mathrm{C}}_{pq}(v+1/2)^p[J'(J'+1)-\Omega'^2]^q - Y^{\mathrm{B}}_{pq}(v+1/2)^p[J''(J''+1)-\Omega''^2]^q\}, \quad (9)$$

where Y^{C}_{pq} and Y^{B}_{pq} denotes the Dunham coefficients for the vibrational ground state of the C state and that for the B state, respectively. The intensity of the respective rotational transition lines in the P, Q, and R branches can be described as

$$\begin{aligned} I_{J',J''} &= h\nu \cdot N_{0,J} \cdot A_{\mathrm{CB}} \\ &\propto \frac{S(J')}{T_r}\exp(-hcB_vJ'(J'+1)/kT_r), \end{aligned} \quad (10)$$

where $N_{0,J'}$ denotes the population of N_2 in the rotational level J' in the vibrational ground state of the C state, A_{CB} the Einstein coefficient of the C-B transition, and $S(J')$

the Hönl-London factors expressed as [22]

$$
\begin{aligned}
S_P(J') &= (J'+1+\Lambda')(J'-1+\Lambda')/(J'+1) \\
S_P(J') &= (2J'+1)\Lambda'^2 / J'(J'+1) \\
S_R(J') &= (J'+\Lambda')(J'-\Lambda')/J' ,
\end{aligned}
\tag{11}
$$

where Λ denotes a quantum number representing the electronic orbital angular momentum about the inter-nuclear axis. The simulation of the observed rotational structure of the C-B (0, 0) transition was performed by changing the rotational temperature T_r as a variable. From the simulation, in which the spectral line width was estimated to be 265 cm^{-1} corresponding to the resolution of the spectrometer, the rotational temperature of N_2 in the C state in the filament was determined to be 450(100) K for all the observed rotational structures recorded at the twelve different input pulse energies in the range between 0.5 and 6.0 mJ/pulse at intervals of 0.5 mJ/pulse. As shown in Fig. 9, the observed rotational structure recorded when the input laser pulse energy was 6 mJ/pulse is well reproduced by the simulation when T_r = 450 K. The constant rotational temperature of 450(100) K in the wide input pulse energy range indicates that the population distribution in the respective rotational levels in the C state of N_2 in the filament is not sensitively influenced by the input laser pulse energy because of the clamping of the laser field intensity in the filament.

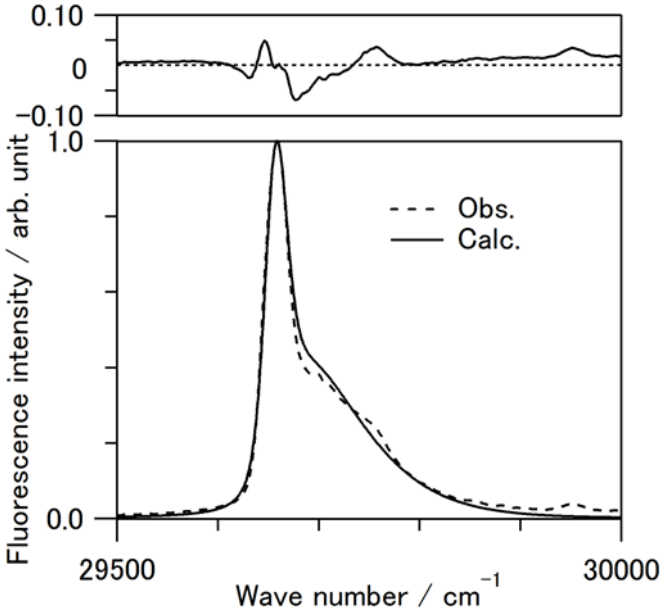

Figure 9. The fluorescence spectra measured from the side of the filament (solid line) when the input laser pulse energy was 6 mJ/pulse, and the simulated spectra (dotted line) at the rotational temperature of 450 K. The solid line in the upper trace represents the residuals (Obs. - Calc.) in the simulation.

4. Conclusion

The backward fluorescence of N_2 from the femtosecond laser filament in air was investigated. The length of the filament defined as the width at the $1/e^2$ intensity of the maximum intensity of the filament was obtained experimentally from the recorded images of the filament. By introducing the one-dimensional amplification model that describes the backward fluorescence intensities emitted from the filament it was confirmed that the backward fluorescence was amplified by the ASE process. Both the vibrational and rotational temperatures of N_2 in the C state, determined from the analysis of the vibrational and rotational structures in the observed spectra of the side fluorescence, were found to take almost constant values in the wide range of the laser pulse energies, which can be ascribed to the intensity clamping process in a laser induced filament.

References

[1] A. Braun, G. Korn, X. Liu, D. Du, J. Squier, G. Mourou, *Opt. Lett.*, **20**, 73 (1995).

[2] H. R. Lange, G. Grillon, J. -F. Ripoche, M. A. Franco, B. Lamouroux, B. S. Prade, A. Mysyrowicz, *Opt. Lett.*, **23**, 120 (1998).

[3] B. La. Fontaine, F. Vidal, Z. Jinag, C. Y. Chien, D. Comtois, A. Desparois, T. W. Johnston, J. -C. Kieffer, H. Pepin, *Phys. Plasmas*, **6**, 1615 (1999).

[4] S. L. Chin, *Femtosecond Laser Filamentation*, Springer, New York (2010).

[5] S. L. Chin, T -J. Wang, C. Marceau, J. Wu, J. S. Liu, O. Kosareva, N. Panov, Y. P. Chen, J. -F. Daigle, S. Yuan, A. Azarm, W. W. Liu, T. Seideman, H. P. Zeng, M. Richardson, R. Li, Z. Z. Xu, *Laser Phys.*, **22**, 1 (2012).

[6] A. Becker, N. Akozbek, K Vijayalakshmi, E. Oral. C. M. Bowden, and S. L. Chin, *Appl. Phys. B*, **73**, 287 (2001).

[7] J. Kasparian, R. Sauerbery, S. L. Chin, *Appl. Phys. B*, **71**, 877 (2000).

[8] C. P. Hauri, W. Kornelis, F. W. Helbing, A. Heinrch, A. Couairon, A. Mysyrowicz, J. Biegert, and U. Keller, *Appl. Phys.* **B**, 79, 673(2004)

[9] C. P. Hauri, A. Guandalini, P. Eckle, W. Kornelis, J. Biegert, and U. Keller, *Opt. Express*, **13**, 7541(2005).

[10] B. Prade, M. Franco, A. Mysyrowicz, A. Couairon, H. Buersing, B. Eberle, M. Krenz, D. Seiffer, O. Vasseur, *Opt. Lett.*, **31**, 2601 (2006)

[11] S. L. Chin, F. Thebgerge, W. Liu, *Appl. Phys. B*, **86**, 477, (2007).

[12] J. Kasparian, M. Rodriguez, G. Mejean, J. Yu, H. Wille, R. Bourayou, S. Frey, Y. -B. Andre, A. Mysyrowicz, R. Sauerbrey, J. -P. Wolf, and L. Woste, *Science*, **301**, 61 (2003).

[13] F. Theberge, N. Akozbek, W. Liu, A. Becker, and S. L. Chin, *Phys. Rev. Lett.*, **97**,

023904 (2006).

[14] M. Rodriguez, R. Sauerbrey, H. Wille, L. Woste, T. Fujii, Y. -B. Andre, A. Mysyrowicz, L. Klingbeil K. Rethmeier, W. Kalkner, J. Kasparian, E. Salmon, J. Yu, and J. -P. Wolf, *Opt. Lett.*, **27**, 772 (2002).

[15] F. Theberge, Q. Luo, W. Liu, S. A. Hosseini, M. Sharifi, and S. L. Chin, *Appl. Phys. Lett.*, **87**, 081108 (2005).

[16] C. D'Amico, A. Houard, M. Franco, B. Prade, A. Mysyrowicz, A. Couairon, and V. T. Tikhonchuk, Phys. Rev. Lett., 98, 235002 (2007).

[17] A. Talebpour, M. A-. Fattah, A. D. Bandrauk, S. L. Chin, *Laser Phys.*, **11**, 68 (2001).

[18] A. Talebpour, S. Petit, S. L. Chin, *Opt. Commun.*, **171**, 285 (1999).

[19] Q. Luo, W. Liu, S. L. Chin, *Appl. Phys. B*, **76**, 337 (2003).

[20] P. S. Cross, W. G. Oldham, *J. Quantum. Electron.*, **QE-11**, 190 (1975).

[21] R. N. Zare, E. O. Larsson, R. A. Berg, *J. Mol. Spec.*, **15**, 117 (1965).

[22] G. Herzberg, *Molecular Spectra and Molecular Structure I: Spectra of Diatomic Molecules*, Prentice-Hall, New York (1939).

Chapter 5

Future perspective

In this thesis, two nonlinear optical phenomena induced in the intense laser field in the vacuum and in the air were investigated. One is investigation of the multiphoton ionization in the EUV wavelength region. The coherent light source in the EUV wavelength region was developed, and the non-resonant two photon ionizations of He irradiated with the seeded FEL pulses and the SASE-FEL pulses were observed. The other is the investigation of the femtosecond laser induced filament. The fluorescence intensity from the filament is interpreted by a model including the spontaneous emission and the stimulated emission, and the laser intensity clamping in the filament is confirmed by the spectral analysis. I would like to propose how I could extend my research in the intense laser field.

In this thesis, the laser intensity at the focus was estimated as 6.3×10^{13} W/cm^2 when the pulse energy, the temporal pulse width and the $1/e^2$ beam radius of the seeded FEL was 10 μJ, 50 fs, and 10 μm, respectively. The Keldysh parameter for He is 18.8 at the intensity of 6.3×10^{13} W/cm^2. If the concave mirror whose focal length is 50 mm is used to focus the FEL pulses instead of the two cylindrical focusing mirrors which were used in this thesis, the laser intensity at the focus will achieved up to 2.5×10^{16} W/cm^2, and the Keldysh parameter will become 0.9. This means the strong field in EUV wavelength region would be formed by using the concave mirror with shorter focal length. The strong field in EUV wavelength region has not been achieved yet, and the formation of the highly charged ions, the tunnel ionization, and the over the barrier ionization would be observed by using the seeded FEL pulses. The investigation of these nonlinear optical phenomena would enable us to investigate the chemical reactions in the intense EUV laser field.

The FEL pulses seeded by high-order harmonics is also promising light source

for the two-color pump-probe experiments in EUV wavelength region. The pump-probe experiment is one of the most useful experiments to examine time dependent ionization process. However, the arrival time jitter between the electron bunch and the synchronized Ti:Sapphire laser pulses, which is usually in the order of sub-ps, limits the temporal resolution of the pump-probe experiments. If the same Ti:Sapphire laser pulse is used to pump the atoms and molecules and to seed the FELs, the temporal jitter between the pump pulse and the prove pulse will be in the order of femtosecond. This means that the FEL seeded by the high-order harmonics enables us to observe the ultrafast phenomena in the intense laser field.

The amplification of the second order harmonics of λ = 61.5 nm was confirmed in this thesis. The amplified second harmonic pulses at 30.7 nm can be used as the coherent seeding light source for the FELs, if there are the undulators in the following part. This is important that further short wavelength could be reached even though accelerator is not feasible to generate such short wavelength. Another technique to generate coherent pulses in shorter wavelength region is called the self-seeding. For EUV and soft X-ray wavelength region, the direct seeding is the promising technique. The seeding light source is usually the high-order harmonics of Ti:Sapphire laser pulses. However, for the X-ray wavelength region, it is difficult to generated the high-order harmonics which is intense enough to seed the FELs. The operation of the seeded FEL in X-ray wavelength region was proposed by the scientists at DESY [1], and reported by the scientists at LCLS [2]. In the self-seeding scheme, the part of the SASE-FEL of narrow bandwidth generated in the first undulator is selected by the X-ray monochromator, and the selected part is amplified in the following undulators. The self-seeded FEL would be a promising light source to investigate the ultrafast reactions of atoms

and molecules in intense laser field.

In this thesis, the amplification of the backward fluorescence intensity indicates the population inversion between $C^3\Pi_u$ and $B^3\Pi_g$ state of N_2 was achieved in the laser filament. The population inversion formed in the femtosecond laser filament enables us to generate the intense ultraviolet laser pulses by seeding the filament with the ultraviolet laser pulses such as the 4th order harmonic of the output of an optical parametric amplifier.

The spectral analysis of the emission spectra enables us to investigate the electronically excited atoms and molecules in the filament. The rotational population distribution of N_2 in the C state becomes clearer if the emission spectra are measured with high spectral resolution. The investigation of the vibrational and the rotational population distribution enables us to realize the mechanism of the excitation of atoms and molecules in the filament.

References

[1] J. Feldhaus, E. L. Saldin, J. R. Scneider, E. A. Schneidmiller, M. V. Yurkov, *Opt. Commun.*, **140**, 341 (1997).

[2] J. Amann, et al., *Nature Photon.*, **6**, 693 (2012).

Acknowledgements

I would like to thank Prof. Kaoru Yamanouchi for his thoughtful supervision over the years, and for giving me the opportunity to participate in wonderful research projects at the RIKEN Harima Branch and at Laval University. I am also deeply grateful to Dr. Atsushi Iwasaki, who gave me great help and a lot of advice for my research on the seeding of FELs, the multiphoton ionization of atoms, and femtosecond laser induced filament. My gratitude also goes out to Dr. Takahiro Sato for his support and guidance on my research at the RIKEN Harima Branch.

I would like to thank Dr. Tetsuya Ishikawa, Dr. Hitoshi Tanaka, Dr. Makina Yabashi, Dr. Mitsuru Nagasono, Dr. Takahiro Watanabe, Dr. Hiromitsu Tomizawa, Dr. Tadashi Togashi, Dr. Shinichi Matsubara, Dr. Yuichi Okayasu, and Dr. Kanade Ogawa at the RIKEN Harima Branch. I would also like to thank Dr. Eiji Takahashi and Dr. Katsumi Midorikawa at the RIKEN Advanced Science Institute, as well as Dr. Koichi Yamakawa and Dr. Makoto Aoyama at the Japan Atomic Energy Agency. I would like to thank the operators of the SCSS test accelerator.

I would like to thank Prof. See Leang Chin, Dr. Ali Azarm, Dr. Sima Hosseini, and Mr. Mario Martin at Laval University, who have invited me for their collaborative research project on the femtosecond laser induced filaments. My visit to Laval University and the collaborative research were a great experience for me.

I would like to thank my colleagues in Prof. Yamanouchi's group, especially Mr. Shun Miura, Mr. Yoshihiro Ide, Mr. Toshiaki Ando, Mr. Seiji Ogami, and Mr. Yuya Morimoto.

Last but not least, I am grateful to my parents for their unconditional support and for their encouragement. I would never have completed my Ph. D study without their immeasurable help.